ASSESSING ECOSYSTEM PHOTOSYNTHETIC POTENTIAL ALONG TWO CALIFORNIA CLIMATE GRADIENTS

by

Sean G. DuBois

A thesis submitted in partial fulfillment of

the requirements for the degree of

Master of Science

(Environment and Resources)

at the

University of Wisconsin-Madison

2015

Acknowledgements

I would like to extend my gratitude to the Desai and Townsend labs, and the NASA HyspIRI project team including Shawn Serbin and Eric Kruger, all of whom assisted in this research and offered supported throughout my graduate career. I would also like to thank my committee members Ankur Desai, Philip Townsend and Adena Rissman, who through classes and individual meetings helped cultivate the ideas expressed in this thesis and always provided invaluable mentorship along the way.

I would like to acknowledge the generous support from the following institutions which provided financial and technical support allowing me to conduct this research: the Wisconsin Space Grant Society Graduate Fellowship, the Nelson Institute for Environmental Studies, ASD inc/ PANalytical Boulder Alexander Goetz Instrument Support Program, and the US National Aeronautics and Space Administration under HyspIRI Prepratory Grant #NNX12AQ28G.

Most of all, I am enormously thankful for the support of all kinds offered by my parents and my wife, Lindsay DuBois, all of whom showed unending patience throughout the research and writing processes throughout my graduate life and beyond.

Abstract

Improving coupled Earth system models of current and future climate requires robust observations that accurately provide parameters and observations for evaluation across spatial scales relevant for the model. Photosynthetic parameters Vc_{max} and J_{max} help to characterize the ability of vegetation to assimilate carbon, a required parameter in most land surface modules of climate models. Gross primary productivity (GPP) is a critical component of the global and regional carbon cycle and discrepancies arise when comparing estimates from various methods. Remote sensing, flux tower data, and field measurements were collected to develop a methodology to estimate the variability in these parameters across diverse landscapes in Southern California and the Sierras, regions experiencing prolonged drought and elevated ozone exposure which is expected to become more common in the future. Preliminary Vc_{max} maps were generated with NASA hyperspectral airborne AVIRIS imagery and produced expected temporal and spatial variability consistent with leaf level estimates. However, Vc_{max} estimated from inverse modeling of flux tower data did not fall in the range found in field measurements for the periods of extensive drought. GPP modeled from the tower data produced high correlation with the imagery, and partial least squares regression offers the ability to generate predictive models of GPP from hyperspectral remote sensing.

Implementation of the methods described in this study on a broad scale will allow for an increased understanding of ecosystem productivity and impacts of drought and air pollution. This expanded dataset can be used to generate effective policy focused on mitigating the effects of drought, air pollution, and climate change.

Table of Contents

Chapter 1: Overview of Flux Towers and Imaging Spectroscopy

Introduction

Increases in atmospheric carbon dioxide are well documented in the past century (Hofmann et al., 2006) and the resulting change in regional climates are predicted to have impacts on local vegetation, especially for Mediterranean climate systems, through changes in precipitation (Breshears et al., 2005). Vegetation shifts resulting from a changing climate have already been quantified in California (Kelly & Goulden, 2008). Meanwhile, there is a need to provide higher accuracy and increased spatial resolution data to models in order to better estimate ecosystem parameters during times of increased vegetative stress (Vargas et al., 2013). Uncertainty exists in our ability to model global photosynthesis and its sensitivity to future climate change.

Recent work by Serbin et al. (2012) has indicated strong evidence for the ability to use hyperspectral imaging collected from high altitude airborne missions to detect photosynthetic rates. Spectroscopy was used to predict leaf metabolic properties Vc_{max}, the maximum rate of carboxylation of the enzyme RuBisCO, and J_{max}, the maximum rate of electron transport necessary to regenerate the RuBP, across ecosystems. Vc_{max} and J_{max} are used to predict photosynthetic capacity using an often employed biochemical model (Farquhar et al., 1980; Farquhar and von Caemmerer, 1982). A robust relationship between spectra and leaf was developed that is applicable across a wide range vegetation types. However, there lacks systematic observations for how leaf level photosynthetic rate constants vary with time and how they scale from leaf to canopy.

In this study, field measurements were made of Vc_{max} to calibrate concurrently collected remote sensing images. Eddy covariance flux tower data – a widely used method to measure ecosystem carbon, water and energy fluxes (Baldocchi and Meyers, 1998) – were used to evaluate the scaling up of leaf level estimates to the canopy. This combination of ecosystem measurement techniques was used to test the hypothesis that imaging spectroscopy is able to simulate spatial and temporal dynamics of scaled Vc_{max} and GPP inferred from flux tower measurements across scrublands and forests of California, and that these parameters reflect response of plants to long-term drought.

Successful inference and scaling estimates of ecosystem parameters across the diverse sites and climate in California will allow for robust methods and models that can be applied to other regions. Furthermore, understanding how these ecosystem traits respond to drought and air pollution have implications for future changes in climate and emission scenarios. Ozone exposure and increased drought severity induced by a changing climate may lead to vegetation mortality and shifts in the regional carbon cycle. Applying improved models which factor in potential effects of pollution and climate change on a broad scale will produce results that can form the foundation for policy recommendations. This can lead to significant political measures focused on mitigating anthropogenic-based stress on vegetation and ensure the vitality of these ecosystems in the future.

Literature Review

Carbon Cycle

Predicting the variability of climate to changes in atmospheric carbon requires a complete understanding of the carbon cycle. Changes in global atmospheric carbon can be confidently estimated and therefore amount of CO2 emissions that remain in the atmosphere (43% on average over the last half century), but are highly variable due to global carbon sinks (Le Quere et al., 2009). Currently, there are significant uncertainties surrounding the variability of carbon sinks which play an important role in influencing future atmospheric CO2 levels (Le Quere et al., 2009). Current modeled feedbacks between atmospheric carbon and terrestrial and aquatic sinks are speculative as there are numerous processes and reservoirs that are unaccounted for, including peat, permafrost soils, fires in addition to certain aquatic mechanisms for storing carbon (Le Quere et al., 2009), which need to be examined to better predict future atmospheric carbon levels.

Global GPP

Gross primary productivity (GPP) is fundamental in understanding the carbon cycle. Globally, GPP for the period 1982-2008 is estimated at 120 Pg C/yr by the IPCC AR4 (Denman et al., 2007), which is within the range of multiple upscaled FLUXNET tower data estimates at 119 ± 6 Pg C/yr (Jung et al., 2011) and 123 ± 8 Pg C/yr (Beer et al., 2010). GPP is highly heterogeneous both spatially and temporally across the globe and within ecosystems. Spatially, GPP correlates with fluxes of carbon, with the largest values occurring in equatorial tropics and smallest in cold and dry environments (Jung et al., 2011). For most of the terrestrial systems globally, interannual variation in NEE is

driven by changes in GPP (Ciais et al., 2005; Jung et al., 2011), while variability predominately caused by ecosystem respiration is restricted to specific tropical areas (Jung et al., 2011). Certain temperate zones including parts of North America exhibit summer GPP values equaling or exceeding rates in the tropics (Jung et al., 2011). It is necessary to develop a strong understanding of GPP variability in temperate areas, as this has significant impacts on the global carbon cycle.

There are large expanses of the globe categorized by vegetation not represented in the FLUXNET database. Additional measurement techniques that cover larger spatial areas are necessary to reduce error on current global and regional GPP estimates, such as remote sensing; remote sensing data from MODIS has been used to create a GPP product with global coverage. Heinsch et al. (2006) compared GPP estimated from tower data and the MODIS product. GPP was calculated for a range of sites using the method described in Desai et al. (2005), similar to the method used in this study. While the MODIS product correlates with tower estimates and summer estimates are similar, MODIS on average overestimated GPP by 20-30%, with periods of transition (particularly leaf onset in the spring) categorized by significant discrepancies between the two methods (Heinsch et al., 2006). Furthermore, MODIS GPP did not capture the variability between sites of similar vegetation type (Heinsch et al., 2006). This study concludes that higher spatial resolution is required to accurately estimate GPP for areas of high productivity and heterogeneous landscapes. Given the limits of current remote sensing techniques to accurately detect spatial or temporal changes across small ecosystem gradients, new instrumentation such as imaging spectroscopy must be explored in order to capture these changes.

GPP and Drought

Regional climate anomalies can cause changes in productivity which are significant on the global scale. Extreme drought in Europe lead to a 30% reduction in GPP which resulted in a pulse of 0.5 Pg C/yr to the atmosphere, equal to how much carbon sequestered in the region over four years (Ciais et al., 2005). Drought conditions were categorized by 6-8 *C increase in mean July temperature, and 50% reductions in annual precipitation, causing NPP for forested areas to drop 16 gC/m^2/month in the summer of 2003 compared to the previous 5 years (Ciais et al., 2005). Examining the impacts of drought on a specific region like the western US has implications on a global scale. Furthermore, understanding specific impacts of the current drought on ecosystem productivity is necessary to assess the effects of expected increased severe weather events brought on by climate change.

Eddy Covariance Flux Towers

Eddy covariance flux towers allow for the assessment of carbon exchange beyond the traditional tools of leaf cuvettes (Collatz et al, 1991), and whole plant (Denmead et al., 1993) and soil (Goulden and Crill 1997) chambers. These methods which are confined to single plants or small areas poorly measure natural variation and often cause a disturbance of the vegetation (Baldocchi, 2003). Flux towers offer the ability to measure net ecosystem exchange (NEE) through the use of micrometeorological theory to interpret vertical wind velocity and scalar carbon concentration fluctuations (Baldocchi et al., 1998).

Baldocchi (2003) assessed the state of eddy covariance flux towers, already widely used with over 180 sites worldwide, and highlighted current concerns and future direction. At the time, concerns over data quality included ability to gapfill accurately, energy balance closure, and sites on complex terrain (Baldocchi, 2003). Research was aimed at addressing such criticism by reevaluating original meteorological theory used to interpret measurements in order to reduce bias errors (Massman and Lee, 2002), and comparing tower estimates with models (Baldocchi and Wilson, 2001; Wilson and Baldocchi, 2001). Future work was expected to estimate gross primary productivity (GPP), net primary productivity (NPP), and ecosystem respiration (Baldocchi, 2003).

Baldocchi (2014) reexamined the growing use of eddy covariance flux tower and evaluated progress that has been made over the past decade. Further opportunities for their use have opened up, as methodologies have been developed to include measurements of trace gasses such as volatile organic carbon compounds, methane, nitrous oxide and aerosols (Baldocchi, 2014). Furthermore, many prospective methods utilizing flux data outlined in Baldocchi (2003) have been achieved, including estimating GPP and ecosystem respiration (Cook et al., 2004; Desai et al., 2005), as well as developing quality controls which allow for confident usage of tower data from complex terrain via low turbulence filtering (Reichstein et al., 2005). The 2014 review calls for expanding collection to a global level through the integration of towers with remote sensing and models, highlighting research involving vegetation indices from hyperspectral reflectance measurements (Ustin et al., 2004).

Vc_{max} inversion

Vc_{max}, the maximum rate of carboxylation in plants, is a necessary parameter to estimate productivity in models employing Farquhar based photosynthesis equations. Flux towers have been used to estimate this photosynthesis parameter via inverse modeling Farquharian photosynthesis equations.

Wolf et al. (2006) estimated leaf area index (LAI), Vc_{max}, the Bal-Berry parameter (m) and substrate-dependent ecosystem respiration rate using carbon and energy fluxes and meteorology variables. This method was solved iteratively, estimating the photosynthesis parameters by comparing a forward run model that predicted ecosystem fluxes to the original measured fluxes. This study focused on a grassland site and measured seasonal variation in the parameters. Groenendijk et al. (2011) followed a similar approach, but used Fluxnet data to include multiple sites and compared modeled LAI to the MODIS LAI product. Field measured LAI was compared to the MODIS and modeled values, with modeled LAI matching the field data better than the MODIS product. Both studies found large seasonal variations in Vc_{max} across all vegetation types and climates. Neither study compared modeled Vc_{max} to field estimates, which is notable as Bonan et al. (2012) showed that values for leaf-level Vc_{max} that yield realistic canopy-scale GPP are often lower than observed in the global synthesis of Kattge et al. (2009). Although actual values from Wolf et al. (2006) and Groenendijk et al. (2011) were not validated and may be questioned due to the findings of Bonan et al. (2012), the predicted seasonal variation does match the field measurements of Wilson et al. (2000). This study measured Vc_{max} over two seasons and observed high Vc_{max} during high productivity and young leaf age with declining values occurring as the growing season wore on and

productivity slowed in the summer and fall, ranging from 7 to 68 μmol $CO_2/m^2/s$ throughout the year for white oak. In order to validate tower based estimates of Vc_{max}, research is needed that compares these modeled values and estimates from field data collected at the leaf level.

Spectroscopy

The ability to estimate GPP from remote sensing data often relies upon work by Monteith (1972), where GPP is described as a function of light use efficiency and photosynthetically active radiation (PAR). The relationship is described in the equation:

$$GPP = \varepsilon * fPAR * PAR \quad \text{(Eq. 1)}$$

where ε is the radiation use conversion efficiency (RUE), fPAR is the fraction of incident PAR absorbed by the canopy, and PAR is that which reaches the canopy (Heinsch et al., 2006). RUE is calculated as a relationship between the maximum RUE for a given biome, temperature, and vapor pressure deficit (VPD). Heinsch et al. (2006) finds discrepancies between GPP estimated by MODIS which follows the above equation and estimates derived from flux tower measurements. Part of the discrepancy lies with biome-wide assumptions that minimize the ability to capture true differences within classified regions.

Serbin et al. (2012) provides a different method for using spectroscopy to calculate specific photosynthesis parameters. Through the use of imaging instruments with high spectral resolution, parameters Vc_{max} and J_{max} were estimated from leaf level spectroscopy. Specific features within the reflected spectrum were used to determine narrow bands that are highly correlated with the desired parameter through the use of

partial least squares regression (PLSR) (Serbin et al., 2012). This method allows for the use of the entire spectrum and has the potential to be used at the canopy scale to determine ecosystem photosynthetic capacity within vegetation types, where previous broad band remote sensing techniques are lacking.

Scaling up the methods developed by Serbin et al. (2012) to the canopy level requires the use of imaging spectroscopy, specifically NASA's Airborne Visible / Infrared Imaging Spectrometer (AVIRIS). This sensor measures reflected solar energy in the 400-2500nm spectral region with 224 spectral bands, with an average bandwidth of 10nm (Vane et al., 1993, Green et al., 1998). AVIRIS, involved in science research since 1987, uses a whisk-broom imaging approach and is often mounted on an ER-2 high altitude aircraft (Vane et al., 1993, Green et al., 1998)). This platform is ideal for this sensor due to its stability, has a low velocity-to-height ratio which improves signal to noise performance, and has a long range allowing for collection of large areas up to 2,100 km from launch site (Vane et al., 1993). The high spectral resolution data has the ability to capture variation in leaf water, chlorophyll, cellulose, lignin, nitrogen, and other leaf constituents (Green et al., 1998), and studies have shown the ability to use this data to map these traits (Ustin and Gamon, 2010; Singh et al., In Review). AVIRIS therefore provides the high resolution remote sensing data necessary to estimate photosynthetic parameters including Vc_{max}.

Chapter 2: Analysis of Imagery and Flux Tower Data

Methods

Site Descriptions

The flux tower sites used in this study comprise two climate gradients, one located in southern California (transecting the San Jacinto Mountains) and the other in central California (rising from the San Joaquin Valley into the Sierra Nevada Mountains). These transects cover changes in elevation, climate, and ecosystems (Figure 2). The use of sites located along these climate gradients allows for numerous ecosystem types to be studied in relatively close space, ensuring the results from this study to be applicable and replicable in other regions. All sites are located within protected areas with limited human disturbance. Flux tower data is extensive for these sites, with data for the southern California transect beginning in 2006, and 2008 for the Sierra climate gradient. Over this time period, these sites have endured wide ranges of annual precipitation as California has experienced drought and non-drought years (Figure 3). Through 2013, however, mean annual temperature has not varied in the same way, with maximum internal variation in temperature at 2 °C and minimum annual temperature variation at some sites less than 0.2 °C.

The southern California climate gradient covers the vegetation types grassland, coastal sagebrush, and an oak-pine forest on the western slope of the San Jacinto Mountains, and pinyon-juniper woodland, chaparral scrubland and desert scrub located on the eastern slope (Kelly & Goulden, 2008), rising from 470 m elevation to 1300 m and back down to 275 m in the desert (Table 1). The Coastal Sagebrush and Grassland sites

are situated within the enclosed Loma Ridge Park with minimal human disturbance outside of ecosystem management activity which includes prescribed burns. These sites have an average rainfall of 150 mm/year with a range of 110 to 750 mm per year, and a mean temperature of 16 °C with variation of 1 °C between years. The Oak-Pine Forest is located within the San Jacinto James Reserve, a University of California Natural Resource System field station, and is used only for research. The mean temperature of 14 °C with 1 °C variation, and mean precipitation at 550 mm/yr with a range of 200 to 1050 mm/yr. The Oak-Pine Forest is encompassed by the Santa Rosa-San Jacinto Mountains National Monument. This national monument located west of Coachella Valley is also the location of the Desert, Desert Chaparral, and Pinyon-Juniper Woodland sites. The Pinyon-Juniper Woodland and Desert Chaparral have a mean annual temperature of 16 °C with 1 °C variation, and a mean precipitation of 100 mm/yr (range of 60 to 200 mm/yr) and 160 mm/yr (80 to 350 mm/yr). The Desert site experiences the highest mean annual temperature of 24 °C with 2 °C variation between years, and mean precipitation of 115 mm/yr (range of 70 to 250 mm/yr).

The Sierra climate gradient is comprised of the three sites Oak-Pine Woodland, Ponderosa Pine, and Mixed Conifer (Figure 1), increasing in elevation from 405 m to 2015 m (Table 1). These sites are situated within the Upper Kings River watershed, located on the western slope of the Sierra Nevada Mountains. The Oak-Pine Woodland is located within the San Joaquin Experimental Range, a US Forest Service enclosed area focused on research of the rangeland ecosystem. This site has a mean annual temperature of 17 °C with 0.5 °C variation between years, and mean annual precipitation of 400 mm/yr, ranging from 100 to 750 mm/yr. The other two Sierra sites, the Ponderosa Pine

and Mixed Conifer forests, are situated in the Sierra National Forest. The Ponderosa Pine forest is the wettest with annual precipitation of 1350 mm/yr, ranging from 500 to 1600 mm/yr with a mean temperature of 15 °C with 1 °C range. The Mixed Conifer site is at the highest elevation and thus the coldest (mean annual temperature: 9 °C with 2 °C internal variability), and mean precipitation of 400 mm/yr (range of 200 to 550 mm/yr).

Remote Sensing Data Collection

The two climate gradients used in the study were flown by the NASA HyspIRI (Hyperspectral Infrared Imaging) campaign, which includes a high altitude ER-2 aircraft collecting imaging spectroscopy and thermal imagery using the AVIRIS (Airborne Visible/Infrared Imaging Spectrometer) and MASTER (MODIS/ Advanced Spaceborne Thermal Emission and Reflection Radiometer Airborne Simulator) sensors (Figure 1). Flights were conducted at least once a season and timed to capture maximum variation in the ecosystems (Figure 4). AVIRIS has a spectral resolution of around 10 nm and covers the electromagnetic range of 414–2447 nm (Vane et al., 1993; Green et al., 1998).

Imagery provided by NASA is level two, meaning it is orthorectified and includes atmospheric corrections, with a spatial resolution of 18 m. The imagery used for this research is the apparent surface reflectance provided from NASA. This product is derived from the radiance measurements from AVIRIS and ATREM (ATmosphere REMoval), a program which determines scaled surface reflectance developed by the Center for the Study of Earth from Space at the University of Colorado, Boulder (Gao et al., 2000).

Preliminary maps of Vc_{max} estimates made from the AVIRIS imagery were provided by members of the project team in order to provide evaluation of the tower estimates in addition to the leaf level measurements. These maps are estimates of leaf

level Vc_{max} at 25 °C for the tower area and surrounding region (Figure 7). Vc_{max} is estimated using the relationship between the photosynthesis parameter and nitrogen per unit lead area (N_{area}) as described in Kattge et al. (2009). Leaf mass per area (LMA) and percent nitrogen can be calculated from the AVIRIS imagery, which is used to estimate N_{area} (Singh et al., In Review).

Field Data Collection

In conjunction with the airborne measurements, ground-based measurements of canopy LAI and clumping, leaf reflectance, temperature, nutrient status, stomatal conductance, and photosynthetic CO_2-response were conducted at two southern CA sites (Coastal Sagebrush and Oak-Pine Forest) and 3 Sierra sites (Oak-Pine Woodland, Ponderosa Pine, and Mixed Conifer Forest) in the spring and summer of both 2013 and 2014. These field measurements were designed to collect data for the calibration of remote sensing products. The field measurements coincided with the HyspIRI overflights.

Leaf level gas exchange, which measures how assimilation varies with leaf internal CO_2 concentration, was measured for all representative species at each site. These measurements allow for the estimation of Vc_{max} and J_{max}, and were conducted using a LI-6400 portable photosynthesis system (Li-Cor Biosciences, Lincoln, NE, USA). For sites with tall vegetation, measurements were taken at the bottom, middle, and top of the canopy, with the youngest fully expanded leaves chosen for measurements, with collection techniques following the field methods described in Serbin et al., 2012.

Flux Tower Data Collection

Eddy covariance flux tower compute net ecosystem exchange (NEE) of trace gases, energy and momentum based on the turbulent conservation equation for fluids (Baldocchi

and Meyers, 1998; Massman and Lee, 2002). The eddy covariance method uses statistical analysis of instantaneous vertical mass flux density to determine their net difference between the canopy-atmosphere interface (Baldocchi, 2003). Estimating half-hourly NEE from CO_2 fluxes is accomplished from the covariance between fluctuations in vertical velocity (w) and the CO_2 mixing ratio ($c = \rho_c/\rho_a$ where ρ_c and ρ_a is the density of air and CO_2, respectively):

$$F = \overline{\rho_a} * \overline{w'c'} \quad \text{(Eq.2)}$$

where overbars signify time averaging and primes as deviation from the mean (Baldocchi, 2003). Positive values denote net CO_2 transfer to the atmosphere (the ecosystem is a carbon source), and negative values as CO_2 into the canopy (ecosystem is a carbon sink).

The theoretical exchange of carbon between canopy and atmosphere is guided by the conservation of mass equation. This equation states that the sum of the local time rate of change of the CO_2 mixing ratio and advection is balanced by the sum of the flux divergence of CO_2 in three dimensions and the biological source-sink strength. Under the assumptions that scalar concentrations and atmospheric wind velocities are steady with time, and the surface is homogenous and flat so that there is no advection, we can write the simplified conservation of mass equation as a balance between vertical flux divergence of CO_2 and the source-sink strength:

$$\frac{\partial F_z}{\partial z} = -S_B(z) \quad \text{(Eq. 3)}$$

where $\partial F_z/\partial z$ is the vertical flux divergence and $S_B(z)$ is the biological source-sink strength (Baldocchi, 2003).

Half-hourly fluxes were computed from the high-frequency (> 10 Hz) measurements at the nine Southern California and Sierra climate gradients sites, which are all managed and processed by Michael Goulden's lab at the University of California-Irvine. Measurements were collected near the top of triangular-cross-section aluminum or steel towers which rise 5 to 10 m above canopy height (Goulden et al., 2012). The high frequency wind velocity measurements were collected with a sonic anemometer (Campbell Scientific CSAT-3) and concentrations of CO_2 and water vapor density with a closed-path Infrared Gas Analyzer (LiCor LI7000) (Goulden et al., 2012). These raw measurements were aggregated into half hour fluxes; other meteorological parameters including air temperature were collected at half hour intervals.

Collection of eddy covariance data on sloped terrain presents issues due to potential vertical movement of air via cold air drainage instead of turbulent flow (Goulden et al., 2006). Our sites, located along an elevation climate gradient and thus sloped terrain, are impacted by this issue and require specific quality control. Daytime fluxes have been shown to be of comparable quality between flat and mountainous terrain (Turnipseed et al., 2002), while fluxes measuring advection can be removed by screening data collected during times of low turbulence (Reichstein et al., 2005). This is accomplished by setting a minimum threshold for friction velocities (u*). Thresholds were determined by choosing the u* value above which respiration was independent of friction velocity. This was conducted on a per site basis at a two year time interval.

In order to generate a complete time series after removing data during the quality control process, we filled missing data points using the Desai-Cook gap filling model

(Cook et al., 2004; Desai et al., 2005). This model was applied to the u* filtered data, utilizing the 30 minute values for NEE, photosynthetically active radiation (PAR), air temperature and site location. The model uses a variable moving-window mean diurnal variation method to estimate missing meteorological data, with the window size depending on the completeness of the dataset.

The Eyring function (Cook et al., 2004; Eyring, 1935) was applied to the filled data to estimate ecosystem respiration (R_{eco}). Gross Primary Productivity (GPP) was modeled from the difference between the 30 minute modeled R_{eco} and the original NEE data. The computed GPP was fit to a Michaelis-Menton reaction rate equation (Falge et al., 2001; Ruimy et al., 1995) in order to fill gaps. The full time series of R_{eco} and GPP was then used to estimate NEE and fill gaps in the original dataset.

Footprint extraction

In order to compare tower data with airborne imagery, the pixels falling within the footprint (area from which the tower senses fluxes) during the time of overflight need to be extracted from the flightline. A one dimensional online footprint model (A Simple Parameterization for Flux Footprint Predictions, 2004) based off the model developed by Kljun et al. (2004) was used to estimate the footprint at each overflight. This simplified model is based off of a wide variety of simulations from a three dimensional model that calculates the trajectories of a Lagrangian model in a backward time frame (Kljun et al., 2002). The simplified model uses estimates for standard deviation of vertical velocity fluctuations, surface friction velocity, measurement height, boundary-layer height, and roughness length, all of which can be derived from the meteorological measurements made at the flux tower, for each overflight. The footprint length was chosen as the

distance from the tower which covers 90% of the vegetation contributing to the flux measured at the tower. The width was calculated as half the total length, so that the footprint was represented as a rectangle beginning from the base of the tower. The rectangle was then divided into squares matching the pixel size (18 m x 18 m), with the latitude and longitude for the center of each used to extract pixels containing the same coordinates from the imagery.

Vc_{max} Inversion

Estimates of Vc_{max} from flux tower data were made from inverse modeling a Farquhar-based photosynthesis model following the method described in Wolf et al. (2006). The model developed in the Wolf study predicts leaf area index (LAI), Vc_{max}, the Ball-Berry parameter (m), and substrate-dependent ecosystem respiration rate. These require inputs from flux tower data including CO_2, energy and water fluxes, in addition to meteorological parameters and soil water content. Output parameters were derived from the inversion of commonly used photosynthesis models, including a mechanistic biochemical model of leaf level carbon uptake (Farquhar et al., 1980), and a modified Ball-Berry equation (Collatz et al., 1991) for solving stomatal conductance. These equations comprised a two layer canopy model (de Pury and Farquhar, 1997) of sunlit and shaded leaves which accounts for direct and diffuse radiation.

Gross assimilation in this model is dependent upon Vc_{max} and J_{max}. J_{max} scales linearly with Vc_{max}, and can therefore be estimated by a scaling factor (2.3) that is an intermediate value for the species found in our study sites, particularly scrub and grassland (Wullschleger, 1993). Assimilation rate (A) is reliant on the CO_2 concentration

within the leaf (Ci), which itself depends on stomatal conductance of the leaf ($gsCO_2$) and leaf surface CO_2 concentration following the equation:

$$Ci = Cs – A/ gsCO_2 \quad \text{(Eq. 4).}$$

Stomatal conductance can by estimated as a function of A, leaf surface relative humidity (rh), leaf surface CO_2 concentration (Cs), minimum conductance (g_0), and a proportionality constant (m) using the Ball-Berry equation (Collatz et al., 1991) as:

$$gs = m*(A*rh)/ Cs + g_0 \quad \text{(Eq. 5).}$$

This equation can be solved using the model by estimating leaf surface CO_2 concentration with the equations:

$$Cs = Ca – A/ gb \quad \text{(Eq. 6)}$$

$$gbCO_2 = \rho_{air}/rbCO_2 \quad \text{(Eq. 7)}$$

with gb (boundary layer conductance) in equation 5 derived using equation 6, where ρ_{air} is moist air density and $rbCO_2$ is boundary layer resistance (Wolf et al., 2006). Due to the interdependency of these equations (A depends on Ci, Ci on gs, and gs on A), they must be solved iteratively. The approach to solving these equations for A described in Baldocchi (1994) was used to find an analytical solution for all equations. Wolf et al. (2006) determined that the correct root that provides a plausible value without an imaginary component is variable under changing environmental conditions. The correct root, chosen by an algorithm from a list provided in Baldocchi (1994), was determined by the program MATLAB (Mathworks Inc., 1999).

Leaf energy balance was solved using a two-sided leaf model (Monteith, 1990; Su et al., 1996), which is necessary to account for the various surfaces exchanging sensible (H) and latent (LE) heat and allows for the exchange of longwave radiation between

sunlit and shaded leaves (Wolf et al., 2006). H and LE are modeled for both sunlit and shaded leaves using standard resistance analog equations with leaf temperature and stomatal conductance estimated from the carbon assimilation submodel (Wolf et al., 2006).

Respiration is accounted for in the model through three components: ecosystem respiration (R_{eco}), the predominant factor, leaf maintenance respiration (Rd), and plant growth respiration (Rg). Root respiration and heterotrophic soil respiration of labile root exudates are the most significant portions of R_{eco} (Chapin and Ruess, 2001). Rd is assumed to scale linearly with Vc_{max} due to its relationship with maintaining proteins during photosynthesis (Reich et al., 1998). Rg includes respiration attributed to stems, roots, leaves, seeds and woody material due to the biochemical synthesis of proteins, carbohydrates, lipids, lignins and organic acids (Amthor, 2000; France and Thornley, 1984; Penning de Vries et al., 1974), and the partitioning of ecosystem growth between roots, stems and leaves was parameterized using field samples (Wolf et al., 2006). Respiration rate was modeled using the substrate-limited approach where the respiration rate is calculated at any timestep as a proportion of the previous 24 hour net assimilation (Wolf et al., 2006). This resulted in respiration following the diurnal cycle for soil temperature with minimum rates occurring immediately at predawn and maxima near sunset (Wolf et al., 2006).

Comparing individual leaf Vc_{max} to flux tower measurements was resolved by upscaling to the canopy level with leaf area index (LAI). Total LAI was partitioned between sunlit and shaded leaves and calculated for each timestep as a function of solar zenith angle and extinction of light through the canopy (Wolf et al., 2006). Successively,

canopy photosynthetic capacity was calculated for sunlit and shaded leaves following equations (15), (22) and (23) in de Pury and Farquhar (1997). Initial Vc_{max} per leaf area at the top of the canopy was integrated over the canopy with the equation:

$$\text{Canopy-}Vc_{max} = LAI * Vc_{max} * (1-e^{-kn})/kn \quad \text{(Eq. 8)}$$

where kn is the N extinction coefficient (a median of reported values in literature (de Pury and Farquhar, 1997; Leuning, 2000) of 0.5 was used), and then partitioned into sunlit and shaded components taking into account the LAI divided into these components (Wolf et al., 2006). Canopy Vc_{max} is linearly scaled with Vc_{max} or LAI, with the other held constant, and is approximately equal to the product of LAI and Vc_{max}.

The specific fluxes of H, LE, and A were summed and multiplied by their respective sun and shade leaf areas to estimate the total canopy fluxes of H, LE, and net ecosystem exchange (NEE) (Wolf et al., 2006). During periods when rain was detected at the flux tower, LE was modeled as the equilibrium evaporation from a wet surface (Monteith, 1990):

$$LEeq = (Rn - G) * s/(s + \gamma) \quad \text{(Eq. 9)}$$

where Rn is net radiation, G is ground head flux (calculated as Rn – H – LE), s is the slope of the saturation vapor pressure-temperature curve, and γ is the psychrometric constant.

In order to determine the collection of ecosystem parameters (LAI, Vc_{max}, **m**, and the rate of dark respiration as a fraction of net carbon assimilation rate) most consistent with the flux data, the modeled fluxes were fit to the measured employing a least squares procedure. Wolf et al. (2006) determined that modeling carbon flux alone would not provide an adequate test the ecosystem parameters due to correlation with LAI and Vc_{max},

but including modeled total outgoing energy (H + LE) which is only weakly determined by Vc_{max} would provide a robust analysis. LAI can then be solved with an estimate of Vc_{max} using the energy balance as absorbed radiation is dependent on leaf area (Sellers et al., 1992). The model then ran iteratively, estimating ecosystem parameters and then modeling fluxes, until it converged upon the minimum sum of squares for the residuals.

The model was computed using filtered and gapfilled NEE along with meteorological data collected at the flux tower site. Estimates were made for all sites in which field measurements were made, which include the Coastal Sagebrush, Oak-Pine Forest, Oak-Pine Woodland, Ponderosa Pine and Mixed Conifer ecosystems. The size of the window period was initially varied to maximize consistency of results while minimizing the amount of gap-filled data, and to test the sensitivity of the model to this factor. The Coastal Sagebrush site was the focus of a multi-year estimation of Vc_{max}, due to the continuity of the data recorded at this site and its close resemblance to the ecosystem used in the Wolf et al. (2006) study.

Imagery-Flux Data Comparison

Footprint cutouts of the AVIRIS imagery was compared against several parameters derived from the flux data, namely NEE, GPP, and the maximum value of NEE and GPP over a two week window centered around the overflight. Taking the maximum value ensured that the actual capacity of the ecosystem was compared with the imagery, as reflectance may align more closely with vegetative capacity than an instantaneous reading (Serbin et al., 2012). Several statistical methods were used to draw comparisons between the two sources, including correlation and linear regression to determine the wavelength regions most important to observing changes in the flux derived parameter.

Standard indices, including Normalized Difference Vegetation Index (NDVI) and Photochemical Reflectance Index (PRI), were calculated and correlated with the flux tower parameters. Normalized Difference Spectral Indices (NDSI), where each band's reflectance value (R) is subtracted by all other bands and divided by their sum (for all possible bands *i* and *j*):

$$NDSI[i,j] = [R_i - R_j]/[R_i + Rj] \quad \text{(Eq. 10).}$$

This index offers the ability to examine all narrow band features and determine their relationship with ecosystem function (Inoue et al., 2008; Ryu et al., 2010). Due to the normalization of each index, values for NDSI range of -1 to 1. This normalization reduces certain undesirable effects of airborne imagery that would otherwise impact comparisons between image files, such as atmospheric disturbance or reflectance artifacts, in addition to standardizing spectral response. Correlation was determined between the resulting output and several flux derived ecosystem parameters, including GPP and NEE and their respective two week maxima, across all sites and within specific vegetative types. Various sets of sites were used when computing the indices, including all sites, only mountain sites (the forested sites with complete canopy cover), and the xeric sites. This categorization of sites was conducted to ensure that methods successful at determining GPP from imagery were not only observing broad differences in vegetation cover, which would be the case when comparing xeric sites with forested sites, but rather determining changes in specific features in the spectra for sites of the same vegetation type.

Partial least squares regression (PLSR) was used to examine the relationship between imagery and tower data. PLSR generates a predictive model of specific

ecosystem traits developed from the AVIRIS data (Wolter et al., 2008; Serbin et al., 2012). This method of creating predictive models has been widely used in remote sensing (Townsend et al., 2003; Ollinger and Smith, 2005; Martin et al., 2008; Wolter et al., 2008), especially when there are more predictor variables than observations, as is often the case when using hyperspectral imagery (Serbin et al., 2012). For this study, all available AVIRIS bands were used as predictor variables, with GPPmax used as the observation. This was conducted with all site data, and subsets based on vegetation type in a similar fashion to the site subsets used with the indices. Verification was performed using a random set of sites to build the model, and the remaining sites data to validate the model.

Results

California Climate

The Southern California transect can be divided into three climate categories: (i) coastal, which includes Coastal Sagebrush and Grassland, (ii) southern interior, consisting of Desert, Desert Chaparral, and Pinyon-Juniper Woodland, and (iii) southern montane which contains the Oak-Pine Forest site. The coastal sites receive most of their annual precipitation in the cooler winter months before an often dry and warm summer. The southern interior sites are the most xeric, with low precipitation usually in the late winter or spring, and intermittent throughout the rest of the year. The southern montane also receives its most significant rainfall in the winter and early spring, but has moderate temperatures relative to the other southern sites.

The Sierra sites are categorized as central interior (Oak-Pine Woodland) and montane (Ponderosa Pine and Mixed Conifer). All sites receive most of the annual precipitation in winter and spring, and at a lesser rate during the rest of the year. The montane sites experience cold winters and moderate summers, while the central interior has moderate winters and warm summers.

California is currently enduring severe drought conditions since the 2012 calendar year (National Drought Mitigation Center, 2014) (Figure 16**)**. This is evident in our data, as annual precipitation has steadily declined since 2011 (Figure 5). All sites in which we examined previous years' data exhibited a decreasing trend in precipitation, with 2013 data often signaling drier conditions that the first year of the drought in 2012. The drought tends to deviate most strongly from previous years' rainfall records in the spring, when the wet season usually delivers a significant portion of the annual precipitation for the southern sites. During drought years, the spring increase in rainfall either did not occur or the magnitude of rainfall drastically decreased.

Ecosystem Carbon Fluxes

The most xeric sites (Desert, Desert Chaparral, and Pinyon-Juniper Woodland) have a bimodal growing season (Figure 4) for 2013 caused from two predominant precipitation periods occurring that year. These events directly resulted in times of increased production. The mesic sites are categorized as having predominately a single peak in productivity occurring in late winter or spring. The single peak is caused by precipitation events and low water demand in the cooler winter months.

Due to the continuous nature of flux tower measurements compared to the irregular remote sensing campaigns, it is necessary to contextualize the imagery with the

eddy covariance measurements. The numerous overflights often were able to categorize annual variability by collecting at periods of both maximum and minimum productivity. However, the sites characterized by maximum GPP occurring in late and early spring (Grassland, Coastal Sagebrush, and Oak-Pine Woodland) reached peak productivity before the first AVIRIS flight of the year. Comparing spectra-derived estimates of photosynthesis must take into account the differences in growing seasons between vegetation types.

Vc_{max} Inversion

Inverse modeling of the Farquhar photosynthesis model using flux tower data provided Vc_{max} and LAI estimates for different vegetation types in the footprint of each flux tower. The model required compete data without gaps, and due to intermittent outages and filtering at all sites, comprehensive estimations of Vc_{max} were conducted at mainly two sites: Coastal Sagebrush and Oak-Pine Forest. Estimates were conducted for days airborne imagery was collected, which also often coincided with field measurements, in order to make comparisons between the various estimation methods. At the Coastal Sagebrush site, within a 5 day window, single day input data was potentially highly variable due to daily changes in light, temperature, and precipitation, with variability reaching 300%. Increasing window sizes from three to four days, and four to five days, did not yield noticeably different results, with maximum variation around 10%. In order to reach a mean estimation that represented the period sampled, window sizes covered at least 4 days provided the original data was relatively complete and required minimal gapfilling.

The Coastal Sagebrush vegetation most closely matches that under which the model was calibrated in the Wolf et al. (2006) study, and therefore this site was chosen for an extensive multi-year analysis of Vc_{max}. Estimates were modeled seasonally from 2010 to the 2013 field campaign (Figure 6**).** Maximum Vc_{max} occurred during the growing season (late winter and early spring) and for 2010 and 2011, reached 186 and 155 µmol $CO_2/m^2/s$, respectively, which is within the range of field measured Vc_{max} in 2013. Non-growing season estimates were much lower and decreased rapidly from peak Vc_{max}**,** with minima occurring during the summer and reaching values 3-5% of the maxima which occurred earlier in the year. In contrast, maximum annual Vc_{max} estimates for 2012 and 2013 are near 10% of the maximum values for 2010 and 2011. Periods of low productivity, the summer and fall for this ecosystem, did occasionally produce estimates of lower Vc_{max} for 2012 and 2013 compared to previous years, but the difference was not as large as the decrease in maximum Vc_{max} (Table 2).

The inverse modeled estimates of Vc_{max} were evaluated with estimates from the leaf level gas exchange and preliminary Vc_{max} estimated from the imagery. Field estimates were conducted in March 2013, with a mean Vc_{max} estimate of 147 with a standard deviation of 71 µmol $CO_2/m^2/s$**,** and ranging from 74 to 300 µmol $CO_2/m^2/s$ for all dominant species (Figure 6)**.** AVIRIS Imagery Vc_{max} estimates ranged from 177 to 179 µmol $CO_2/m^2/s$ between April and March 2013. Thus, there is a discrepancy between the inverse model and the other estimation methods, as the minimum field recorded Vc_{max} (72 µmol $CO_2/m^2/s$**)** was 380% greater than the maximum modeled Vc_{max} for 2013.

In order to confine the model, Leaf Area Index (LAI) was constrained from MODIS estimates for the Coastal Sagebrush and Oak-Pine Forest sites in an attempt to

improve the performance of the model. The same input values were used, with the addition of MODIS LAI and removing the LAI estimation by the model. For the Coastal Sagebrush site, MODIS LAI was 41% of the estimated LAI (mean annual LAI for MODIS was 1.06, whereas the model estimated 2.56). Field estimates of LAI were 1.9 for March 2013, while MODIS estimated 0.8, and the model 2.7. The Oak-Pine Forest site saw similar differences between MODIS and model results, with spring MODIS estimated LAI at 64% of the model estimates (1.6 and 2.5, respectively). The addition of the constrained LAI into the model saw an increase in estimated leaf level Vc_{max}. At the Coastal Sagebrush site for the chosen dates, the model Vc_{max} increased 540% with the confined LAI, and a 34% increase in Sum of Squares between predicted and observed fluxes. The confined LAI model Vc_{max} estimates averaged 425.46 µmol $CO_2/m^2/s$, compared to the previous mean of 66.51 µmol $CO_2/m^2/s$ across all dates sampled. Similarly at the Oak-Pine Forest, Vc_{max} increased 170% when using MODIS LAI. However, there was not a noticeable difference in resulting Sum of Squares (SS). Although the increased Vc_{max} yielded acceptable carbon flux estimates when compared to field data as apparent with the similar SS value, it failed to accurately yield acceptable sensible heat flux measurements, which was 50% of the values from the unconstrained LAI model run and the field data.

Footprint Extraction

Footprint estimates were estimated for each tower site at the time of overflight. The maximum fetch contribution, the distance from the tower for which that vegetation had the highest contribution to the overall flux, varied for each overflight but followed the trend for being closer to shorter towers, and the mean was 88 m. The distance for which

90% of the measured flux is accounted for also followed the trend of with the taller towers having higher values, in addition to sites with a heterogeneous landscape, such as an oak savanna, having larger footprints (non-forested sites mean: 169m, forested and savanna sites mean: 274 m). The half hour wind trends were similar to the overall annual pattern that influenced field plots, and in conjunction with the calculated fetch lengths generally support the comparison of tower and field data due to the overlapping of measured vegetation and calculated footprints.

Imagery-Flux Data Comparison

Each pixel located within a flux tower footprint was averaged in order to compare to the corresponding tower data. This resulted in 41 total data points, spread across all nine sites and covering high and low productivity times of the year (Figure 4). To ensure correlation was not spurious or dependent upon temporal factors including day of year and time of day, each AVIRIS band was correlated with the tower parameters including meteorological data, fluxes, and temporal categorization parameters. Meteorological and temporal parameters correlated poorly with all bands (maximum $|r| < 0.5$), while ecological factors had a strong relationship with bands in the visible and both short wave infrared (SWIR) wavelengths ($|r| > 0.5$). While NEE and GPP measurements taken before, during, and after the airborne collection correlated well with the imagery, maximum GPP from a two week window around the overflight (GPPmax) showed the strongest relationship across visible ($r = -0.77$) and both SWIR regions ($r = -0.76$ and $r= -0.80$, respectively).

Band ratios were used to determine the success of traditional imagery analysis at capturing the ecological change within and between sites. Normalized difference

vegetation index (NDVI; wavelengths [850-650]/[850+650]) had a strong relationship with tower ecological parameters when looking across all vegetation types ($r = 0.82$ for GPPmax, $r > 0.72$ for instantaneous GPP and NEE) (Figure 8), but fails to capture intra-site variation (Figure 9). Additionally, Photochemical Reflectance Index (PRI; wavelengths [531-570]/[531+570]) does not correlate with GPP across sites ($r = 0.34$). Chlorophyll estimation (wavelengths [(1/700)-(1/850)-0.1515]/0.01517) has moderate correlation with tower ecological parameters ($0.62 < |r| < 0.72$).

In contrast to traditional, broad spectrum indices, normalized difference spectral indices were explored to examine potential narrow band features. Broad areas of the spectrum correlated well with tower ecological parameters ($|r| > 0.6$), including GPPmax and NEE (Figure 10**).** In order to determine relationships between imagery and specific vegetation types, and have an acceptable sample size, forested vegetation sites (Oak-Pine Forest, Ponderosa Pine, and Mixed Conifer) were binned into a category named mountain sites, resulting in a sample size of 20. Applying the same method of correlating NDSI with various ecological parameters, the broad areas of correlation fall out, while specific NDSI bands maintain high correlation ($r > 0.7$) (Figure 11). These indices of high correlation generally occurred where the two bands creating the NDSI were close in number, with absolute value of correlation greater than 0.85 for wavelength combinations 520 and 510, 790 and 770, and 2130 and 2110. Similarly, xeric sites (Desert, Desert Chaparral, and Pinyon-Juniper) were subsampled (n=12) and correlations determined for ecological parameters and NDSI. Similar to the mountain sites, indices of nearby wavelengths were often highly correlated ($|r| > 0.85$); however, broad spectrum indices including the SWIR 1 and NIR maintained high correlation (Figure 12).

To test the predictive capabilities of the imagery for ecological parameters, partial least squares regression was used to build a model to estimate such properties. Models focused on estimating GPPmax due to this parameter having the highest correlation with individual bands, but similar parameters were also tested, including GPP during overflight and GPP anomaly (GPPmax – site annual mean GPP). Model results are comprised of 100 simulations, with final R^2, root mean square error (RMSE), and bias values as model averages. The model shows ability to estimate GPPmax across all sites and vegetation types, and when confined to forested sites only where there is often a full canopy year round due to the presence of evergreen species (Figure 15). PLS coefficients indicate the significance of specific wave bands in predicting the given variable; these plots indicate that often specific features across the entire spectrum have a strong influence on predictive capability (Figure 13 and 14**)**. Furthermore, similar wavelengths from the visible, NIR, and SWIR 1 and 2 are influential in both the all site and mountain subset model runs. Examining predictive capabilities beyond GPPmax, models were built for estimating half hourly GPP coinciding with the overflight, and the model again produced robust results with a similar R^2 value (Table 3). In order to remove the site specific GPPmax values, GPP anomaly (GPPmax – site GPP average for 2013) for mountain sites was used as the predicting variable, leading to reduced R^2 and root mean square error (RMSE), but increased the model bias.

Discussion

Vc_{max} Inversion

There is a clear discrepancy between the flux data and the other two methods for estimating Vc_{max}. Although there are no field measurements in 2011, the Wolf estimated Vc_{max} is around the expected value for the Coastal Sagebrush site during springtime. Even throughout 2012 and 2013, there is variation in the Vc_{max} estimate, but it does not reach levels often associated with viable ecosystems. Comparing this to the AVIRIS map of Vc_{max}, the spatial heterogeneity of Vc_{max} does not include such low estimates (Figure 7). Our analysis shows that drought reduces the ability of the models used in the inversion to correctly predict ecosystem photosynthetic properties, which is concurrent with previous studies (Breshears et al., 2005; Vargas et al., 2013). Given the decrease in Vc_{max} estimates during the transition between pre-drought to drought conditions, we suggest that the Wolf approach does not accurately estimate Vc_{max} during periods of high water stress for our sites. However, Vc_{max} estimates are correlated with GPP modeled from flux data ($r=0.70$), and although the estimates do not reach levels measured in the field, the model still captures annual changes in productivity. Therefore, this method for estimating Vc_{max} from tower data is not suitable under the current climate conditions.

After constraining the model with MODIS LAI estimates, the Vc_{max} for the Coastal Sagebrush site results increased dramatically, but exceeded field and imagery estimates. The increase in Oak-Pine Forest estimates resulted in values closer to field estimates. These increases in Vc_{max} estimates are directly tied to a reduction in LAI, as the scaling from the leaf level to the canopy or flux tower level directly depends on site LAI (see Methods for equation), with leaf level Vc_{max} inversely related to the LAI

estimate. The increase in Vc_{max} at times resulted in comparable estimates, but with increased sum of square values, or an inability to forward model accurate energy fluxes.

Flux Tower based Vc_{max} results from this study are not consistent with field estimates, but are within the range of the results in Wolf et al. (2006), where estimates ranged from 4.51 to 19.92 μmol $CO_2/m^2/s$. Groenendijk et al. (2011) used similar inverse modeling methods to estimate the parameter and for a wide range of vegetation types observed modeled estimates ranging from 13.1 to 141.6 μmol $CO_2/m^2/s$. While these studies observed seasonal shifts in Vc_{max}, the estimated values were not evaluated with field measurements. Our results where modeled Vc_{max} is below field estimates is similar to results in Bonan et al. (2012), which concluded that leaf-level Vc_{max} values that yield realistic GPP at the canopy scale are lower than observed in the global synthesis of Kattge et al. (2009) for most ecosystems. Therefore, inverse modeling has a tendency to underestimate Vc_{max} when comparing to field data. However, the dramatic seasonal variation of Vc_{max} is observed in both field (Wilson et al., 2000) and model based (Wolf et al., 2006; Groenendijk et al., 2011), suggesting that annual variability of Vc_{max} found in models is accurate although specific values may not be, which agrees with the findings from this study.

Eddy Covariance Flux Tower

The flux tower data provides a long-term view that places the airborne field experiment imagery into context. This data shows the diversity of ecosystem types, suggesting these methodologies can be applied to a broader spatial area under various climatic conditions. This study has demonstrated the ability to examine changes across ecosystems and within vegetation types.

The multi-year tower dataset provides background for the significance of the current drought and the impact it has had on Californian vegetation. All sites have seen a decrease in annual GPP, with most sites peak GPP reduced as well. Furthermore, peak productivity for the southern sites and some Sierra sites moved to earlier in the year when it was cooler and wetter. A common theme among sites is the drastic reduction in late season GPP. Peak productivity is often affected, but the largest decrease occurs in the summer and fall due to the reduced spring rainfall that historically provided some of the necessary moisture during the times of high water demand in the summer months. Thus, both maximum and minimum GPP are reduced on average due to the ongoing drought, while there are exceptions. Although productivity has declined, there is evidence of resilience to the drought for certain sites. All three xeric sites (Desert, Chaparral, and Pinyon-Juniper) experience a rapid increase in productivity after a rain event occurring in early September 2013 which is the maximum value for the year, and above or near the 2012 maxima. Furthermore, the mountain sites do not see a noticeable decrease in maximum productivity occurring in the spring even after a large reduction in GPP during the previous summer.

Imagery-Flux Data Comparison

The results of the NDSI and PLSR indicate a strong ability to estimate ecosystem parameters from the AVIRIS imagery. These results specifically rely on specific features present in the collected spectroscopy, which have been used to estimate ecological properties when using narrowband spectroscopy (Zarco-Tejada et al., 2001; Singh et al., In review). These features are expressed as high correlation between narrowband NDSI and GPPmax (Figure 10-12), as the traits represented by these features affect

productivity. Moreover, there are similar features which are significant in the PLS model, including the red edge (690-750 nm) which is known to shift under various stress conditions (Vogelmann et al., 1993). These features and their changes are associated with specific elements in leaf structure that influence plant productivity, and therefore GPP on a canopy scale, and therefore these changes can be used to develop predictive models as shown in this study.

Several ecological parameters derived from tower data correlated strongly with the imagery, including GPP, NEE, and GPPmax. Examining the correlation with individual bands and with NDSI reveals GPPmax had the strongest relationship with the imagery. This suggests that the imagery can capture not only instantaneous properties, but features related to ecosystem capacity. Conditions for an individual day impacts instantaneous fluxes, but is unlikely to change leaf photosynthetic ability. Therefore examining a two week maximum may be a more reliable indicator of the capacity of the vegetation and what is reflected and captured by the sensor.

Subsampling forested sites demonstrated the predictive ability of imaging spectroscopy beyond conventional broad band remote sensing. While NDSI demonstrated high correlation between broad ranges of indices, traditional broad indices such as NDVI also had high correlation with GPP. Focusing on forested sites, there is a reduction in correlation between NDVI and GPP. This loss of correlation is also present in the broad ranges of NDSI. However, narrowband indices for wavelengths in which specific features appear maintained the high correlation, in addition to the predictive capability of the PLS model when confined to forest sites. The relationship between broad band indices such as NDVI and ecological properties tend to diminish with LAI above 3 and 4 (Ollinger and

Smith 2005), values typical in closed canopy ecosystems. Imaging spectroscopy with high spectral resolution is able to maintain high correlation in these vegetation types, and provides the opportunity to accurately map ecosystem properties where broadband sensors are limited.

The features producing strong correlation between NDSI and GPP for both the mountain site model and the model generated using all site data, along with the PLS coefficients (Figure 13 and 14), are located in close proximity to wavelength regions known to be associated with key leaf physiological properties. For the SWIR regions, RuBisCo has known spectral absorption features around wavelengths 1500, 1680, 1740, 1940, 2050, 2170, 2290, and 2470 nm (Elvidge, 1990), while significant wavelengths in the Vc_{max} model presented in Serbin et al. (2012) occur at 1510, 1680, 1760, 1940, 2210, and 2490 nm. These coincide with high correlation values for narrow-band NDSI for mountain sites wavelengths 1712 to 1772, 2058 and 2290 nm, and significant mountain sites PLS coefficients between 1562 and 1752, and between 2278 and 2307. Furthermore, wavelengths in the green reflectance region (around 510 nm) are of high correlation in NDSI and produce significant PLS coefficients. This region is associated with the xanthophyll cycle pigments (Gamon et al., 1997). The features driving the high correlation in NDSI and significant PLS coefficients have physiological meaning, suggesting a theoretical background to the empirical model.

Conclusion

Flux tower measurements were employed to evaluate the ability to scale Vc_{max} estimates from the leaf to the canopy level. The inverse modeling technique to derive Vc_{max} from the flux tower data was inadequate at predicting reasonable estimates due to the ongoing

drought in the western U.S. When constraining the model with external estimates of LAI from MODIS, values of Vc_{max} were comparable to field estimates for the Oak-Pine Forest, although forward modeled fluxes did not match the measured fluxes. Future work may involve introducing field estimates of LAI to the model.

Flux tower measurements and modeled GPP offer important observations which can inform remote sensing data collection due to the continuous collection. The results from the NDSI and PLSR indicate known specific features within the vegetation spectra are driving the correlation between the tower data and the imagery. Calibrating the imagery with the tower data allow for estimates traditionally made from eddy covariance flux tower data to be expanded to broader areas via remote sensing. Long-term and high spatial resolution of ecosystem metabolism data is capable with satellites equipped with sensors similar to the HyspIRI spectrometers.

Chapter 3: Research implications in the context of air quality policy

The methods and results presented in this paper outline the ability to monitor productivity on a regional to global scale. With the focus of the research on California over the past years, this research quantifies the impact of drought on several vegetation types. The increased understanding of ecosystems through the use imaging spectroscopy and flux tower data will allow for increased knowledge on the impacts of severe weather events and anthropogenic emissions. A key component of interdisciplinary research is incorporating scientific results into policy recommendations (Charlson et al., 1992; Hughes et al., 2003). Therefore, the next step of this research is to describe the challenges facing the ecosystems analyzed in this study and examine how policy focused on these issues can be augmented through the use of these methods and result. The challenges include drought and poor air quality, specifically ozone, which currently affect the productivity of California vegetation; these stressors will be exacerbated regionally and globally with increased severe weather events associated with climate change.

History of Air Quality Policy

Degraded air quality has long been known to have detrimental impacts on human health (Mitman, 2005) and on vegetation (Treshow, 1968; Boyle et al., 1997). State and federal governments moved to address these issues with the implementation of air quality standards in the 1950s (California) and 1970s (nationally). These standards, or maximum allowed atmospheric concentrations for each pollutant, are implemented on the national level by the US Environmental Protection Agency (EPA), while additional measures may

be enacted by the states if perceived necessary and allowed by the EPA. Understanding the manner in which these standards are set is critical when developing scientific methods designed at influencing policy.

The EPA began regulating air pollutants after the 1970 amendment to the Clean Air Act (CAA) mandated that the EPA develop national air-quality standards, which in turn set up the National Ambient Air Quality Standards (NAAQS) (Rosenbaum 2014). Standards were implemented in 1971 for carbon monoxide, nitrogen dioxide, ozone, particle pollution, and sulfur dioxide, with lead standards implemented in 1978. All of these standards have been reexamined every decade to ensure they reflect the most current scientific findings.

The method for developing new standards includes a lengthy period for gathering the most recent data on the issue, and a public comment period among other steps (see Figure 18). This review process relies heavily on the current state of scientific literature on the specific pollutant, such as in the Integrated Science Assessment and the Risk/Exposure Assessment. In order to adequately incorporate and understand the science of the studies, EPA relies on the Clean Air Scientific Advisory Committee (CASAC) that is dedicated to independently analyzing the current literature. CASAC is composed of a diverse set of scientists and physicians from disciplines related to air pollution and chosen by the EPA Administrator (Scientific Advisory Board, 2014), allowing the committee to integrate a wide variety of research into the recommendation they provide to the Administrator.

CASAC is commissioned to provide an independent evaluation of the critical scientific literature (Jasanoff 1990), and compiles a report for every standards review,

which the 1977 CAA amendment requires every five years though historically occurs around once a decade. The report includes an analysis of the current literature from the disciplines of atmospheric physics and chemistry, controlled human exposure studies, epidemiology, toxicology, and ecology. The studies focused on human health comprise the information used to create a primary standard, while the studies examining the effect of ozone on the environment, including vegetation and visibility, fall under the secondary standard. However, all previous reviews of the ozone standard have resulted in the implementation of a grouping of these two standards, so that there is one ozone level to prevent harmful effects on both humans and the environment. Furthermore, CASAC reviews the staff paper prepared by the Office of Air Quality Planning and Standards. The staff paper is designed to combine science and policy by identifying key studies relevant to the pollutant's impact on public health, and CASAC must confirm the scientific validity before the report can assist the administrator in deciding on the new standard.

In addition, states can request from the EPA permission to set their own standards that are above the air quality standard enforced nationally. California is one of the few states that has implemented their own policies, as the state has been at the forefront of implementing air standards aimed at improving public health and indirectly mitigated effects on vegetation. The progressive nature of California environmental policy is in part a response to the state's persistent poor air quality driven by population, energy use, climate, and topographic features. Therefore, California implemented standards statewide in 1959 set by the CA Department of Public Health aimed at curbing total suspended particulates, photochemical oxidants, sulfur dioxide, nitrogen dioxide, and carbon

monoxide (Air Resources Board, 2009). Furthermore, the California Air Resources was established in 1967 to determine and enforce new air quality standards based of a review of the current literature on air pollution.

The California Air Resources Board (ARB), the organization within the California Environmental Protection Agency responsible for regulating air pollution, has consistently set their own ozone standards at lower concentrations than the EPA level. The ARB employs a similar system to determining air quality standards as the EPA. The scientific literature review is completed and presented in a staff report. Members of the committee generating this report include ARB staff scientists and contractors, comprising a knowledgeable team to conduct an independent review similar to that of CASAC (Drechsler, 2014). This staff report includes recommendations on where the standard should be set. These recommendations and their bases are peer-reviewed by the Air Quality Advisory Committee, whose members are appointed by the Office of the President of the University of California. This group contains experts in health sciences, exposure assessment, monitoring methods, and atmospheric sciences, to confirm the validity of the staff report and recommendations (Air Resources Board, 2013). Similar to the EPA, the recommendations from the report are used by the Board and chairman to determine the level at which the new standard is set.

Although both the national and state standard setting process include similar scientific reviews, there are often discrepancies in the resulting standards between the two agencies. Differences may arise due to unique political pressure and acceptable uncertainty levels for each agency, but potentially also arising from data and literature with vague or conflicting results. Therefore clear results from an extensive dataset would

help to reduce inconsistencies in the interpretation of scientific research. The use of imaging spectroscopy to estimate changes in ecosystem productivity can provide such a dataset and influence policy regarding drought, climate change, and air pollutants such as ozone.

Drought and Climate Change

Over the past 3 years California has experienced its most severe drought conditions in a century, and perhaps a millennia (Griffin and Anchukaitis, 2014). The impact such conditions have on the ecosystem are apparent in the results from this research and previous work in the same area and around the globe (Ciais et al., 2005; Vargas et al., 2013).

Drought is not an uncommon occurrence in the Western US. Over the past 15 years, a significant portion (20% or greater) of California has experienced extreme drought as categorized by the US Drought Monitor for at least 6 months on 4 separate occasions (Figure 16), and on five occasions over 60% of the state experienced at least moderate drought, totaling nearly 6 years of drought (National Drought Mitigation Center, 2014).

Although drought is a common occurrence in the western US, increases in severity due to climate change may have profound impacts on the vegetation (Bonan, 2008). Generating a database of current conditions is vital to understand ecosystem change under severe stress in the future. Flux towers provide high temporal resolution data from which estimates of productivity can be derived. However, this data is restricted to the area near the tower, and assumptions need to be made when attempting to scale to the regional level that is significant to the global carbon cycle. Novel methods of

estimating regional to global productivity is required to better understand changes in productivity and resulting impacts on the carbon cycle.

Climate change has implications on vegetation similar to that of drought with the potential to significantly change ecosystems. California has experienced climatic changes which have altered vegetation in the past (Kelly and Goulden, 2008), where plant distribution shifted along elevation gradients in response to warming and increased precipitation variability over a 30 year time period ending in 2007. Changes in climate are expected to continue and cause increased stress on local flora, specifically in California (Gershunov et al., 2009) where increased temperature leads to increased water stress particularly in montane ecosystems less adapted for such conditions compared to xeric areas. These changes are largely a result of anthropogenic carbon emissions (IPCC, 2014). While increased atmospheric concentrations lead to higher rates of carbon uptake, there is a leveling off due to diminishing returns (Cramer et al., 2001), and climatic results due to increased atmospheric CO_2 such as increased temperature and precipitation variability may negate any positive effects of carbon "fertilizing."

In my opinion, policies must be enacted that prepare for and mitigate impacts of future climate change. This can be accomplished by directly reducing anthropogenic CO_2 emissions and by reducing human disturbance of at-risk ecosystems. California compiled recent scientific literature on climate change focusing on the state into the Climate Change Research Plan, currently a draft intended to influence climate change policies. It is comprised of policy framework, historical climate change, climate change science, and social science associated with climate change (Climate Action Team, 2014). The climate science included in the Plan spans the disciplines of agriculture, industry, natural lands,

oceans, human health, and water. The Plan calls for research in the next five years to "develop a better understanding of forest and woodland ecosystem dynamics" (Climate Action Team, 2014). Furthermore, importance is put on research to increase forest carbon storage while managing for resilient forests. Finally, policies taking this research into account will use a cost-benefit analysis on ecosystem services, particularly forest carbon.

The methods used in this research make use of the high temporal data gathered from eddy covariance flux towers to generate predictive models using hyperspectral data. These models, applied to a larger scale, have the potential to monitor productivity throughout a region. Furthermore, when applied to a satellite, these models would be able to make predictions on a global scale. In addition to estimating photosynthetic parameters across space as inputs for vegetation models, these methods would monitor changes in photosynthesis on a global scale capturing impacts drought, other climatic stressors, and anthropogenic emissions have on productivity. This increased understanding of vegetation will better inform management techniques. Results from this study have demonstrated the effects of drought on vegetation and the ability to capture these changes using flux towers and remote sensing. Furthermore, an expanded application of these methods will be able to answer the request in the California Climate Change Research Plan Draft to better understand California forests. The dataset created by frequent hyperspectral images will be able to capture changes in forest productivity, determine the ability to sequester carbon, and explore conditions that impact this process. This application has the potential to generate more successful policy based on empirical results.

Ozone

Ozone is formed from sunlight initiating a reaction between hydrocarbons and nitrogen oxides, the latter which is emitted from industrial processes. Ground level ozone is the principal component of smog, which is prevalent in densely populated areas including Los Angeles (Vitousek et al., 1997), and is detrimental to human health. For example, the gas can cause breathing problems and/or asthma, damages vegetation, reduces visibility, and can damage rubber, fabric, and other materials (Rosenbaum 2014). Ozone is relevant to this study as exposure of the pollutant to plants results in reduced productivity (Fuhrer et al., 1997; Ashmore, 2005). This pollutant is particularly of importance to California due to the unique combination of population, climate, and geography of the state. The methods for estimating productivity described in this study can be used to directly determine impacts of ozone on vegetation on a broad scale and assist with implementation of necessary standards to curb this effect.

Ozone standards require compliance by all counties in the US as not to exceed specified atmospheric concentrations. Ozone, initially regulated as oxidants, is one of the six criteria pollutants managed and monitored under the NAAQS. Individual states with EPA approval, such as California, may implement their own standards but they must at least abide by the national standards as well. For ozone, the national standard is an 8-hour average atmospheric concentration, and is currently set at 0.075 ppm.

Ozone is the most prevalent pollutant in California in terms of people affected and the frequency and severity of standard violations (Palmer 1993). Recent studies estimate that a third of California residents live in areas where the ozone concentration rises above

the national standard; the numbers are much worse in the San Joaquin valley, where only a quarter of the residents live in areas in compliance with the standard (Barboza 2014). The high number of non-attainment areas—counties that have ozone levels which exceeded the standard—stem from climate, topography, and population. Los Angeles is surrounded by mountains, preventing emissions generated by the city from escaping. Furthermore, Southern California is dry in the summer months which coincides with the high ozone concentration season. Therefore ozone created in the basin is confined by the topography and without rain to remove the pollution from the air, the ozone concentration increases and may exceed the air quality standard. The same situation is true for the Central Valley, which is confined by the Sierras, has little summer rain, and has major metropolitan centers such as San Francisco that emit ozone causing pollutants that lay stagnant in the valley. These areas often experience some of the highest ozone concentrations in the nation (Figure 17) (Air Now, 2014).

Since 1975, the ozone standards set by the ARB has been set at the "highest level of ozone that can be present without adverse health effects" (Air Resources Board, 2013). However, ozone standards have not included a level designed specifically for vegetation. This is an important oversight because plant exposure to ozone has indirect impacts on humans by impacting agriculture and reducing productivity and therefore ecosystem services (Fares et al., 2013). The EPA 2014 ozone review examined a potential secondary "welfare" standard that would focus on long term exposure, which is a better indicator of potential harm to vegetation (Massman, 2004). Conclusions from the review suggest a welfare standard would not noticeably reduce plant ozone exposure for most areas of the US, with California one of the exceptions (EPA, 2014). This review examined research

mostly confined to individual plot studies rather than empirical results on the regional scale for which the policy suggestions were applied. This is an example where hyperspectral imagery could be used in a similar manner described in this study to examine actual changes in productivity across wide areas exposed to high ozone concentrations. Specific ecosystems could then be targeted for different standards depending on the sensitivity of the vegetation so that specific policy could be implemented at a finer resolution (state or county level) than the broad regions used in the EPA review.

Conclusion

Imaging spectroscopy calibrated with eddy covariance flux tower data has been demonstrated to accurately estimate productivity where traditional broadband techniques could not. Applying these methods to a larger scale via a future satellite will allow for reliable global productivity estimation. This dataset in conjunction with frequent monitoring of change will provide the necessary information to improve a variety of ecosystem related policy. This includes understanding impacts of drought on a regional scale, and tuning climate change policy to maximize carbon sequestration by limiting ozone exposure. Unique challenges will arise under global change, and in order to create effective policy, it will be critical to understand the current and future state of global ecosystems.

Literature Cited

A Simple Parameterization for Flux Footprint Predictions (2004), Available at: http://footprint.kljun.net [Accessed 10 September 2014].

Air Now (2014), Office of Air Quality Planning and Standards, US Environmental Protection Agency, Available at: http://www.airnow.gov [Accessed 12 March 2014].

Air Resource Board (2013), California Ambient Air Quality Standards. California Air Resources Board, Available at: http://www.arb.ca.gov/research/aaqs/aaqs.htm [Accessed 23 March 2014]

Amthor, J. S. (2000), The McCree-de Wit-Penning de Vries-Thornley respiration paradigms: 30 years later, *Annals of Botany*, *86*(1), 1-20, doi:10.1006/anbo.2000.1175.

Anonymous (2005), *Using the Li-6400 portable gas exchange system, Version 5*, Lincoln, NE, USA: Li-Cor Biosciences Inc.

Ashmore, M. R. (2005), Assessing the future global impacts of ozone on vegetation, *Plant Cell and Environment*, *28*(8), 949-964, doi:10.1111/j.1365-3040.2005.01341.x.

Baldocchi, D. (1994), An analytical solution for coupled leaf photosynthesis and stomatal conductance models, *Tree Physiology*, *14*(7-9), 1069-1079.

Baldocchi, D. (2014), Measuring fluxes of trace gases and energy between ecosystems and the atmosphere – the state and future of the eddy covariance method, *Global Change Biology*, *20*(12), 3600-3609, doi:10.1111/gcb.12649.

Baldocchi, D., and T. Meyers (1998), On using eco-physiological, micrometeorological and biogeochemical theory to evaluate carbon dioxide, water vapor and trace gas fluxes over vegetation: a perspective, *Agricultural and Forest Meteorology*, *90*(1-2), 1-25, doi:10.1016/s0168-1923(97)00072-5.

Baldocchi, D. D. (2003), Assessing the eddy covariance technique for evaluating carbon dioxide exchange rates of ecosystems: past, present and future, *Global Change Biology*, *9*(4), 479-492, doi:10.1046/j.1365-2486.2003.00629.x.

Baldocchi, D. D., and K. B. Wilson (2001), Modeling CO2 and water vapor exchange of a temperate broadleaved forest across hourly to decadal time scales, *Ecological Modelling*, *142*(1-2), 155-184, doi:10.1016/s0304-3800(01)00287-3.

Barboza, D. (2014), One-third in state still live where air does not meet U.S. standards, *Los Angeles Times*.

Beer, C., et al. (2010), Terrestrial Gross Carbon Dioxide Uptake: Global Distribution and Covariation with Climate, *Science*, *329*(5993), 834-838, doi:10.1126/science.1184984.

Bonan, G. B. (2008), Forests and climate change: Forcings, feedbacks, and the climate benefits of forests, *Science*, *320*(5882), 1444-1449, doi:10.1126/science.1155121.

Bonan, G. B., K. W. Oleson, R. A. Fisher, G. Lasslop, and M. Reichstein (2012), Reconciling leaf physiological traits and canopy flux data: Use of the TRY and FLUXNET databases in the Community Land Model version 4, *Journal of Geophysical Research-Biogeosciences*, *117*, 19, doi:10.1029/2011jg001913.

Boyle, C. A., L. Lavkulich, H. Schreier, and E. Kiss (1997), Changes in land cover and

subsequent effects on lower fraser basin ecosystems from 1827 to 1990, *Environmental Management*, *21*(2), 185-196, doi:10.1007/s002679900017.

Breshears, D. D., et al. (2005), Regional vegetation die-off in response to global-change-type drought, *Proceedings of the National Academy of Sciences of the United States of America*, *102*(42), 15144-15148, doi:10.1073/pnas.0505734102.

Chapin, F. S., and R. W. Ruess (2001), Carbon cycle - The roots of the matter, *Nature*, *411*(6839), 749-752, doi:10.1038/35081219.

Charlson, R. J., S. E. Schwartz, J. M. Hales, R. D. Cess, J. A. Coakley, J. E. Hansen, and D. J. Hofmann (1992), CLIMATE FORCING BY ANTHROPOGENIC AEROSOLS, *Science*, *255*(5043), 423-430, doi:10.1126/science.255.5043.423.

Ciais, P., et al. (2005), Europe-wide reduction in primary productivity caused by the heat and drought in 2003, *Nature*, *437*(7058), 529-533, doi:10.1038/nature03972.

Climate Action Team (2014), California Climate Change Research Plan: Public Discussion Draft, California Environmental Protection Agency.

Collatz, G. J., J. T. Ball, C. Grivet, and J. A. Berry (1991), Physiological and environmental-regulation of stomatal conductance, photosynthesis and transpiration - a model that includes a laminar boundary-layer, *Agricultural and Forest Meteorology*, *54*(2-4), 107-136, doi:10.1016/0168-1923(91)90002-8.

Cook, B. D., et al. (2004), Carbon exchange and venting anomalies in an upland deciduous forest in northern Wisconsin, USA, *Agricultural and Forest Meteorology*, *126*(3-4), 271-295, doi:10.1016/j.agrformet.2004.06.008.

Cramer, W., et al. (2001), Global response of terrestrial ecosystem structure and function to CO2 and climate change: results from six dynamic global vegetation models, *Global Change Biology*, *7*(4), 357-373, doi:10.1046/j.1365-2486.2001.00383.x.

Denman, K. L., and G. Brasseur (2007), Couplings Between Changes in the Climate System and Biogeochemistry, in *Climate Change 2007: the Physical Science Basis*, edited by S. Solomon, D. Qin, M. Manning, M. Marquis, K. Averyt, M. M. B. Tignor, H. L. Miller and Z. L. Chen, pp. 499-587, Cambridge Univ Press, New York.

Denmead, O. T., F. X. Dunin, S. C. Wong, and E. A. N. Greenwood (1993), Measuring water-use efficiency of eucalypt trees with chambers and micrometeorological techniques, *Journal of Hydrology*, *150*(2-4), 649-664, doi:10.1016/0022-1694(93)90130-2.

De Pury, D. G. G., and G. D. Farquhar (1997), Simple scaling of photosynthesis from leaves to canopies without the errors of big-leaf models, *Plant Cell and Environment*, *20*(5), 537-557, doi:10.1111/j.1365-3040.1997.00094.x.

Desai, A. R., P. V. Bolstad, B. D. Cook, K. J. Davis, and E. V. Carey (2005), Comparing net ecosystem exchange of carbon dioxide between an old-growth and mature forest in the upper Midwest, USA, *Agricultural and Forest Meteorology*, *128*(1-2), 33-55, doi:10.1016/j.agrformet.2004.09.005.

Drechsler, D. (2014, April 21), Telephone interview.

EPA (2014), Welfare Risk and Exposure Assessment for Ozone, Office of Air Quality Planning and Standards, Publication No. EPA-452/R-14-005c.

Elvidge, C. D. (1990), Visible and near-infrared reflectance characteristics of dry plant materials, *International Journal of Remote Sensing*, *11*(10), 1775-1795.

Eyring, H. (1935), Activated complex in chemical reactions, *Journal of Chemical Physics*, *3*, 107-115, doi:10.1063/1.1749604.

Falge, E., et al. (2001), Gap filling strategies for defensible annual sums of net ecosystem exchange, *Agricultural and Forest Meteorology*, *107*(1), 43-69, doi:10.1016/s0168-1923(00)00225-2.

Fares, S., R. Vargas, M. Detto, A. H. Goldstein, J. Karlik, E. Paoletti, and M. Vitale (2013), Tropospheric ozone reduces carbon assimilation in trees: estimates from analysis of continuous flux measurements, *Global Change Biology*, *19*(8), 2427-2443, doi:10.1111/gcb.12222.

Farquhar, G. D., and S. v. Caemmerer (1982), Modelling of photosynthetic response to environmental conditions, *Encyclopedia of plant physiology. New series. Volume 12B. Physiological plant ecology. II. Water relations and carbon assimilation. [Lange, O.L.; Nobel, P.S.; Osmond, C.B.; Ziegler, H. (Editors)]*, 549-587.

Farquhar, G. D., S. V. Caemmerer, and J. A. Berry (1980), S biochemical-model of photosynthetic CO_2 assimilation in leaves of C-3 species, *Planta*, *149*(1), 78-90, doi:10.1007/bf00386231.

France, J., and J. H. M. Thornley (1984), Mathematical models in agriculture, *Mathematical models in agriculture.*, xi + 335pp.

Fuhrer, J., L. Skarby, and M. R. Ashmore (1997), Critical levels for ozone effects on vegetation in Europe, *Environmental Pollution*, *97*(1-2), 91-106, doi:10.1016/s0269-7491(97)00067-5.

Gamon, J. A., L. Serrano, and J. S. Surfus (1997), The photochemical reflectance index: an optical indicator of photosynthetic radiation use efficiency across species, functional types, and nutrient levels, *Oecologia*, *112*(4), 492-501, doi:10.1007/s004420050337.

Gao, B. C., M. J. Montes, Z. Ahmad, and C. O. Davis (2000), Atmospheric correction algorithm for hyperspectral remote sensing of ocean color from space, *Applied Optics*, *39*(6), 887-896, doi:10.1364/ao.39.000887.

Gershunov, A., D. R. Cayan, and S. F. Iacobellis (2009), The Great 2006 Heat Wave over California and Nevada: Signal of an Increasing Trend, *Journal of Climate*, *22*(23), 6181-6203, doi:10.1175/2009jcli2465.1.

Goulden, M. L., R. G. Anderson, R. C. Bales, A. E. Kelly, M. Meadows, and G. C. Winston (2012), Evapotranspiration along an elevation gradient in California's Sierra Nevada, *Journal of Geophysical Research-Biogeosciences*, *117*, doi:10.1029/2012jg002027.

Goulden, M. L., and P. M. Crill (1997), Automated measurements of CO2 exchange at the moss surface of a black spruce forest, *Tree Physiology*, *17*(8-9), 537-542.

Goulden, M. L., G. C. Winston, A. M. S. McMillan, M. E. Litvak, E. L. Read, A. V. Rocha, and J. R. Elliot (2006), An eddy covariance mesonet to measure the effect of forest age on land-atmosphere exchange, *Global Change Biology*, *12*(11), 2146-2162, doi:10.1111/j.1365-2486.2006.01251.x.

Green, R. O., et al. (1998), Imaging spectroscopy and the Airborne Visible Infrared Imaging Spectrometer (AVIRIS), *Remote Sensing of Environment*, *65*(3), 227-248, doi:10.1016/s0034-4257(98)00064-9.

Griffin, D., and K. J. Anchukaitis (2014), How unusual is the 2012–2014 California

drought?, *Geophysical Research Letters*, 1944-8007, doi:10.1002/2014GL062433

Groenendijk, M., et al. (2011), Seasonal variation of photosynthetic model parameters and leaf area index from global Fluxnet eddy covariance data, *Journal of Geophysical Research-Biogeosciences*, *116*, 18, doi:10.1029/2011jg001742.

Heinsch, F. A., et al. (2006), Evaluation of remote sensing based terrestrial productivity from MODIS using regional tower eddy flux network observations, *IEEE Transactions on Geoscience and Remote Sensing*, *44*(7), 1908-1925, doi:10.1109/tgrs.2005.853936.

Hofmann, D. J., J. H. Butler, E. J. Dlugokencky, J. W. Elkins, K. Masarie, S. A. Montzka, and P. Tans (2006), The role of carbon dioxide in climate forcing from 1979 to 2004: introduction of the Annual Greenhouse Gas Index, *Tellus Series B-Chemical and Physical Meteorology*, *58*(5), 614-619, doi:10.1111/j.1600-0889.2006.00201.x.

Hughes, T. P., et al. (2003), Climate change, human impacts, and the resilience of coral reefs, *Science*, *301*(5635), 929-933, doi:10.1126/science.1085046.

Inoue, Y., J. Penuelas, A. Miyata, and M. Mano (2008), Normalized difference spectral indices for estimating photosynthetic efficiency and capacity at a canopy scale derived from hyperspectral and CO2 flux measurements in rice, *Remote Sensing of Environment*, *112*(1), 156-172, doi:10.1016/j.rse.2007.04.011.

IPCC (2014), *Climate Change 2014: Impacts, Adaptation, and Vulnerability. Part A: Global and Sectoral Aspects. Contribution of Working Group II to the Fifth Assessment Report of the Intergovernmental Panel on Climate Change* [Field, C.B., V.R. Barros, D.J. Dokken, K.J. Mach, M.D. Mastrandrea, T.E. Bilir, M. Chatterjee, K.L. Ebi, Y.O. Estrada, R.C. Genova, B. Girma, E.S. Kissel, A.N. Levy, S. MacCracken, P.R. Mastrandrea, and L.L. White (eds.)]. Cambridge University Press, Cambridge, United Kingdom and New York, NY, USA, 1132 pp.

Jackson, L. P. (2009), Process for Reviewing National Ambient Air Quality Standards, *NAAQS Review Process Memo*, US Environmental Protection Agency

Jasanoff, S. (1990), *The Fifth Branch: Science Advisors as Policymakers*. Harvard University Press.

Jung, M., et al. (2011), Global patterns of land-atmosphere fluxes of carbon dioxide, latent heat, and sensible heat derived from eddy covariance, satellite, and meteorological observations, *Journal of Geophysical Research-Biogeosciences*, *116*, 16, doi:10.1029/2010jg001566.

Kattge, J., W. Knorr, T. Raddatz, and C. Wirth (2009), Quantifying photosynthetic capacity and its relationship to leaf nitrogen content for global-scale terrestrial biosphere models, *Global Change Biology*, *15*(4), 976-991, doi:10.1111/j.1365-2486.2008.01744.x.

Kelly, A. E., and M. L. Goulden (2008), Rapid shifts in plant distribution with recent climate change, *Proceedings of the National Academy of Sciences of the United States of America*, *105*(33), 11823-11826, doi:10.1073/pnas.0802891105.

Kljun, N., P. Calanca, M. W. Rotach, and H. P. Schmid (2004), A simple parameterisation for flux footprint predictions, *Boundary-Layer Meteorology*, *112*(3), 503-523, doi:10.1023/b:boun.0000030653.71031.96.

Kljun, N., M. W. Rotach, and H. P. Schmid (2002), A three-dimensional backward lagrangian footprint model for a wide range of boundary-layer stratifications, *Boundary-Layer Meteorology*, *103*(2), 205-226, doi:10.1023/a:1014556300021.

Le Quere, C., et al. (2009), Trends in the sources and sinks of carbon dioxide, *Nature Geoscience*, *2*(12), 831-836, doi:10.1038/ngeo689.

Leuning, R. (2000), Estimation of scalar source/sink distributions in plant canopies using Lagrangian dispersion analysis: Corrections for atmospheric stability and comparison with a multilayer canopy model, *Boundary-Layer Meteorology*, *96*(1-2), 293-314, doi:10.1023/a:1002449700617.

Martin, M. E., L. C. Plourde, S. V. Ollinger, M. L. Smith, and B. E. McNeil (2008), A generalizable method for remote sensing of canopy nitrogen across a wide range of forest ecosystems, *Remote Sensing of Environment*, *112*(9), 3511-3519, doi:10.1016/j.rse.2008.04.008.

Massman, W. J. (2004), Toward an ozone standard to protect vegetation based on effective dose: a review of deposition resistances and a possible metric, *Atmospheric Environment*, *38*(15), 2323-2337, doi:10.1016/j.atmosenv.2003.09.079.

Massman, W. J., and X. Lee (2002), Eddy covariance flux corrections and uncertainties in long-term studies of carbon and energy exchanges, *Agricultural and Forest Meteorology*, *113*(1-4), 121-144, doi:10.1016/s0168-1923(02)00105-3.

MathWorks Inc. (1999), *Matlab*, Prentice Hall, Upper Saddle River, N. J.

Mitman, G. (2008) *Breathing Space: How Allergies Shape Our Lives and Landscapes*. Yale University Press.

Monteith, J. L. (1972), Solar-radiation and productivity in tropical ecosystems, *Journal of Applied Ecology*, *9*(3), 747-766, doi:10.2307/2401901.

National Drought Mitigation Center (2014), United States Drought Monitor, Available at: http://droughtmonitor.unl.edu/ [Accessed 12 September 2014].

Ollinger, S. V., and M. L. Smith (2005), Net primary production and canopy nitrogen in a temperate forest landscape: An analysis using imaging spectroscopy, modeling and field data, *Ecosystems*, *8*(7), 760-778, doi:10.1007/s10021-005-0079-5.

Palmer, T. (1993), *California's Threatened Environment: Restoring the Dream*, Island Press, Covelo, CA.

Penningd.Fw, Brunstin.Ah, and H. H. Vanlaar (1974), Products, requirements and efficiency of biosynthesis - quantitative approach, *Journal of Theoretical Biology*, *45*(2), 339-377.

Reich, P. B., M. B. Walters, D. S. Ellsworth, J. M. Vose, J. C. Volin, C. Gresham, and W. D. Bowman (1998), Relationships of leaf dark respiration to leaf nitrogen, specific leaf area and leaf life-span: a test across biomes and functional groups, *Oecologia*, *114*(4), 471-482, doi:10.1007/s004420050471.

Reichstein, M., et al. (2005), On the separation of net ecosystem exchange into assimilation and ecosystem respiration: review and improved algorithm, *Global Change Biology*, *11*(9), 1424-1439, doi:10.1111/j.1365-2486.2005.001002.x.

Rosenbaum, W. A. (2014) *Environmental Politics and Policy- 9th ed*, CQ Press, Los Angeles, CA.

Ruimy, A., P. G. Jarvis, D. D. Baldocchi, and B. Saugier (1995), CO 2 fluxes over plant

canopies and solar radiation: a review, *Advances in Ecological Research, 26*, 1-63, doi:10.1016/s0065-2504(08)60063-x.

Ryu, Y., D. D. Baldocchi, J. Verfaillie, S. Ma, M. Falk, I. Ruiz-Mercado, T. Hehn, and O. Sonnentag (2010), Testing the performance of a novel spectral reflectance sensor, built with light emitting diodes (LEDs), to monitor ecosystem metabolism, structure and function, *Agricultural and Forest Meteorology*, *150*(12), 1597-1606, doi:10.1016/j.agrformet.2010.08.009.

Scientific Advisory Board (2014), List of Candidates for the Chartered Clean Air Scientific Advisory Committee, *Environmental Protection Agency Science Advisory Board Staff*. Available at: http://yosemite.epa.gov/sab/sabpeople.nsf/ [Accessed 09 Jan. 2015]

Sellers, P. J., J. A. Berry, G. J. Collatz, C. B. Field, and F. G. Hall (1992), Canopy reflectance, photosynthesis, and transpiration .3. A reanalysis using improved leaf models and a new canopy integration scheme, *Remote Sensing of Environment*, *42*(3), 187-216, doi:10.1016/0034-4257(92)90102-p.

Serbin, S. P., D. N. Dillaway, E. L. Kruger, and P. A. Townsend (2012), Leaf optical properties reflect variation in photosynthetic metabolism and its sensitivity to temperature, *Journal of Experimental Botany*, *63*(1), 489-502, doi:10.1093/jxb/err294.

Singh, A., S. P. Serbin, B. E. McNeil, C. C. Kingdon, P. A. Townsend, Retrieval of canopy foliar chemical and morphological traits and their uncertainty using imaging spectroscopy, *In Review.*

Su, H. B., K. T. Paw, and R. H. Shaw (1996), Development of a coupled leaf and canopy model for the simulation of plant-atmosphere interaction, *Journal of Applied Meteorology*, *35*(5), 733-748, doi:10.1175/1520-0450(1996)035<0733:doacla>2.0.co;2.

Townsend, P. A., J. R. Foster, R. A. Chastain, and W. S. Currie (2003), Application of imaging spectroscopy to mapping canopy nitrogen in the forests of the central Appalachian Mountains using Hyperion and AVIRIS, *Ieee Transactions on Geoscience and Remote Sensing*, *41*(6), 1347-1354, doi:10.1109/tgrs.2003.813205.

Treshow, M. (1968), Impact of air pollutants on plant populations, *Phytopathology*, *58*(8), 1108-&.

Turnipseed, A. A., P. D. Blanken, D. E. Anderson, and R. K. Monson (2002), Energy budget above a high-elevation subalpine forest in complex topography, *Agricultural and Forest Meteorology*, *110*(3), 177-201, doi:10.1016/s0168-1923(01)00290-8.

Ustin, S. L., and J. A. Gamon (2010), Remote sensing of plant functional types, *New Phytologist*, *186*(4), 795-816, doi:10.1111/j.1469-8137.2010.03284.x.

Ustin, S. L., D. A. Roberts, J. A. Gamon, G. P. Asner, and R. O. Green (2004), Using imaging spectroscopy to study ecosystem processes and properties, *Bioscience*, *54*(6), 523-534, doi:10.1641/0006-3568(2004)054[0523:uistse]2.0.co;2.

Vane, G., R. O. Green, T. G. Chrien, H. T. Enmark, E. G. Hansen, and W. M. Porter (1993), The airborne visible infrared imaging spectrometer (AVIRIS), *Remote Sensing of Environment*, *44*(2-3), 127-143, doi:10.1016/0034-4257(93)90012-m.

Vargas, R., et al. (2013), Drought Influences the Accuracy of Simulated Ecosystem Fluxes: A Model-Data Meta-analysis for Mediterranean Oak Woodlands, *Ecosystems*, *16*(5), 749-764, doi:10.1007/s10021-013-9648-1.

Vitousek, P. M., J. D. Aber, R. W. Howarth, G. E. Likens, P. A. Matson, D. W. Schindler, W. H. Schlesinger, and D. Tilman (1997), Human alteration of the global nitrogen cycle: Sources and consequences, *Ecological Applications*, *7*(3), 737-750, doi:10.2307/2269431.

Vogelmann, J. E., B. N. Rock, and D. M. Moss (1993), Red edge spectral measurements from sugar maple leaves, *International Journal of Remote Sensing*, *14*(8), 1563-1575.

Wilson, K. B., and D. D. Baldocchi (2001), Comparing independent estimates of carbon dioxide exchange over 5 years at a deciduous forest in the southeastern United States, *Journal of Geophysical Research-Atmospheres*, *106*(D24), 34167-34178, doi:10.1029/2001jd000624.

Wilson, K. B., D. D. Baldocchi, and P. J. Hanson (2000), Spatial and seasonal variability of photosynthetic parameters and their relationship to leaf nitrogen in a deciduous forest, *Tree Physiology*, *20*(9), 565-578.

Wolf, A., K. Akshalov, N. Saliendra, D. A. Johnson, and E. A. Laca (2006), Inverse estimation of Vc(max), leaf area index, and the Ball-Berry parameter from carbon and energy fluxes, *Journal of Geophysical Research-Atmospheres*, *111*(D8), 18, doi:10.1029/2005gd005927.

Wolter, P. T., P. A. Townsend, B. R. Sturtevant, and C. C. Kingdon (2008), Remote sensing of the distribution and abundance of host species for spruce budworm in Northern Minnesota and Ontario, *Remote Sensing of Environment*, *112*(10), 3971-3982, doi:10.1016/j.rse.2008.07.005.

Wullschleger, S. D. (1993), Biochemical limitations to carbon assimilation in C(3) plants - a retrospective analysis of the A/Ci curves from 109 species, *Journal of Experimental Botany*, *44*(262), 907-920, doi:10.1093/jxb/44.5.907.

Zarco-Tejada, P. J., J. R. Miller, T. L. Noland, G. H. Mohammed, and P. H. Sampson (2001), Scaling-up and model inversion methods with narrowband optical indices for chlorophyll content estimation in closed forest canopies with hyperspectral data, *IEEE Transactions on Geoscience and Remote Sensing*, *39*(7), 1491-1507, doi:10.1109/36.934080.

Appendix A: Tables

Table 1: List of sites including their location, climate, and dominant vegetation.

Site	Latitude	Longitude	Elev. (m)	Mean Annual Precipitation (mm/yr)	Mean Temperature (°C)	Vegetation
Desert	33.652	-116.372	275	115	24	Desert Perennials and Annuals
Desert Chaparral	33.596	-116.445	1300	100	16	Desert Shrubland
Pinyon-Juniper Woodland	33.592	-116.448	1280	100	16	Pinyon, Juniper
Grassland	33.737	-117.695	470	150	16	Annual Grassland
Coastal Sagebrush	33.734	-117.696	475	150	16	California Sage, White Sage, Malosma
Oak-Pine Forest	33.803	-116.753	1710	550	14	Oak, Pine, Cedar
Oak-Pine Woodland	37.079	-119.720	405	400	17	Foothills Pine, Oak, Annual Grasses
Ponderosa Pine	37.029	-119.256	1160	1350	15	Ponderosa Pine, Oak
Mixed Conifer	37.067	-119.195	2015	400	9	White Fir, Pine, Cedar

Table 2: Timeseries of Vcmax estimates from inverse modeling with tower data. The Day of Year (DOY) column is composed of the range of dates used to model a single Vc_{max} over that time period. Values denoted with (*) are results using MODIS LAI. Vc_{max} values are in µmol $CO_2/m^2/s$.

Site	Year	DOY	LAI	Vcmax	SS	MODIS LAI	Vcmax*	SS*
Oak-Pine Forest	2011	111-113	2.7	15.9	16.0	1.4	67.3	15.8
	2012	110-112	2.5	10.4	2.9	1.5	31.4	2.9
	2013	86-88	2.4	18.0	0.4	1.7	41.8	0.4
	2013	108-110	2.4	22.0	3.1	1.8	38.1	3.2
Coastal Sage	2010	30-34	2.5	41.1	5.1	0.9	510.0	10.0
	2010	60-63	2.4	186.3	11.4	1.6	294.2	16.0
	2010	99-105	2.3	146.8	15.9	1.6	232.1	25.9
	2010	150-153	2.8	20.3	1.5	0.9	632.5	2.3
	2010	183-186	2.9	8.2	0.6	0.7	693.5	0.7
	2010	241-243	2.4	30.8	1.3	0.5	711.8	1.3
	2011	107-110	2.3	154.9	12.7	1.8		
	2011	124-127	2.4	37.7	5.6	1.4		
	2011	151-154	2.9	19.7	2.4	1.1	555.9	4.9
	2011	257-260	3.0	3.6	1.9	0.5		
	2011	349-352	2.4	16.2	2.6	0.7		
	2012	67-70	2.6	8.4	21.3	0.7	38.6	22.4
	2012	108-111	2.8	17.5	6.2	1.2		
	2012	150-153	2.9	7.3	3.0	0.7		
	2012	249-253	3.0	1.5	18.0	0.5		
	2012	356-359	2.4	2.3	4.9	0.3		
	2013	46-50	2.6	12.6	40.8	1.1		
	2013	83-86	2.7	13.2	2.0	0.8	617.1	3.0
	2013	104-106	2.5	15.2	0.4	0.7		
	2013	141-145	3.0	2.0	3.8	0.5		

Table 3: All are values are model-averaged over the 100 runs. Multiple forms of the parameter Gross Primary Productivity (GPP) were used to test the predictive capabilities of the model, and all resulted in strong fits. GPP anomaly is the difference between GPPmax and the annual GPP mean for the site.

Variable	**R^2**	**RMSE**	**BIAS**
Gpp During (All)	0.861	1.512	-0.025
Gppmax (All)	0.852	1.406	-0.368
Gppmax (Mtn)	0.865	1.648	-0.136
Gpp Anomaly (Mtn)	0.889	1.186	-0.251

Appendix B: Figures

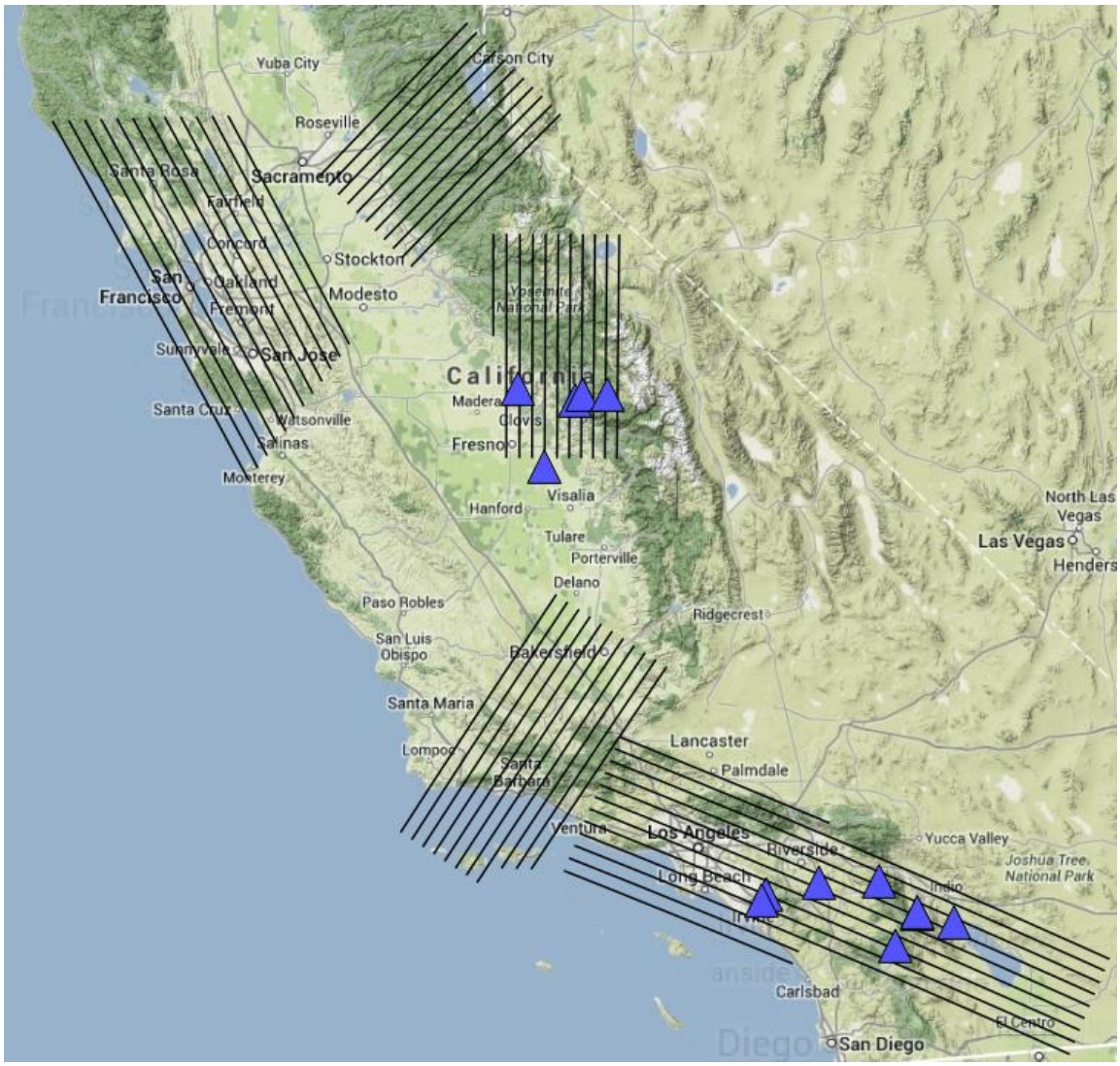

Figure 1: Location of the core study sites found within the five HyspIRI campaign flight boxes. The southern sites comprise the southern California climate gradient, while the northern lie along the Sierra gradient. All tower sites are included in the HyspIRI overflights

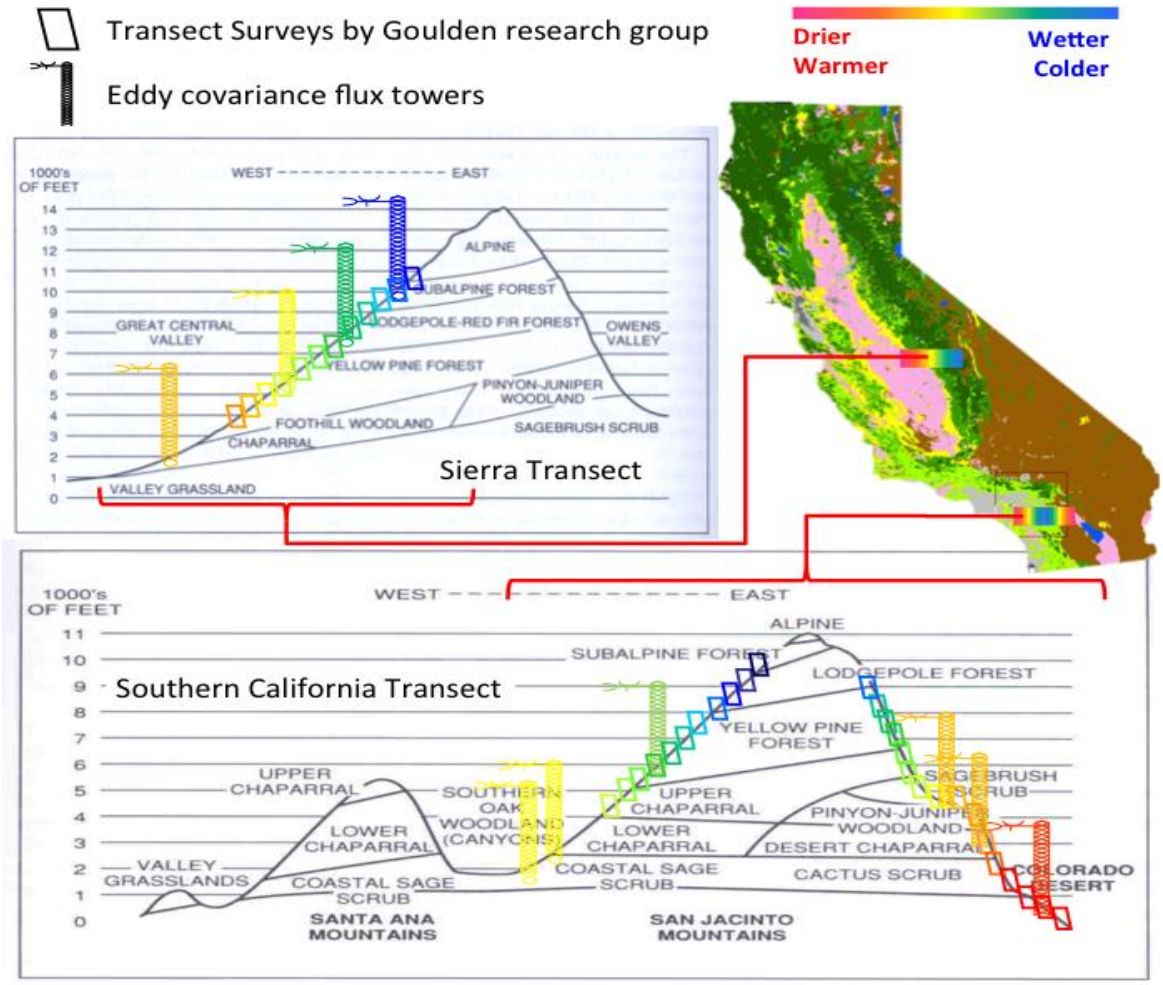

Figure 2: The two transects cover numerous ecosystems along two separate elevation climate gradients. Flux tower sites are positioned along each transect to measure each distinct vegetation type.

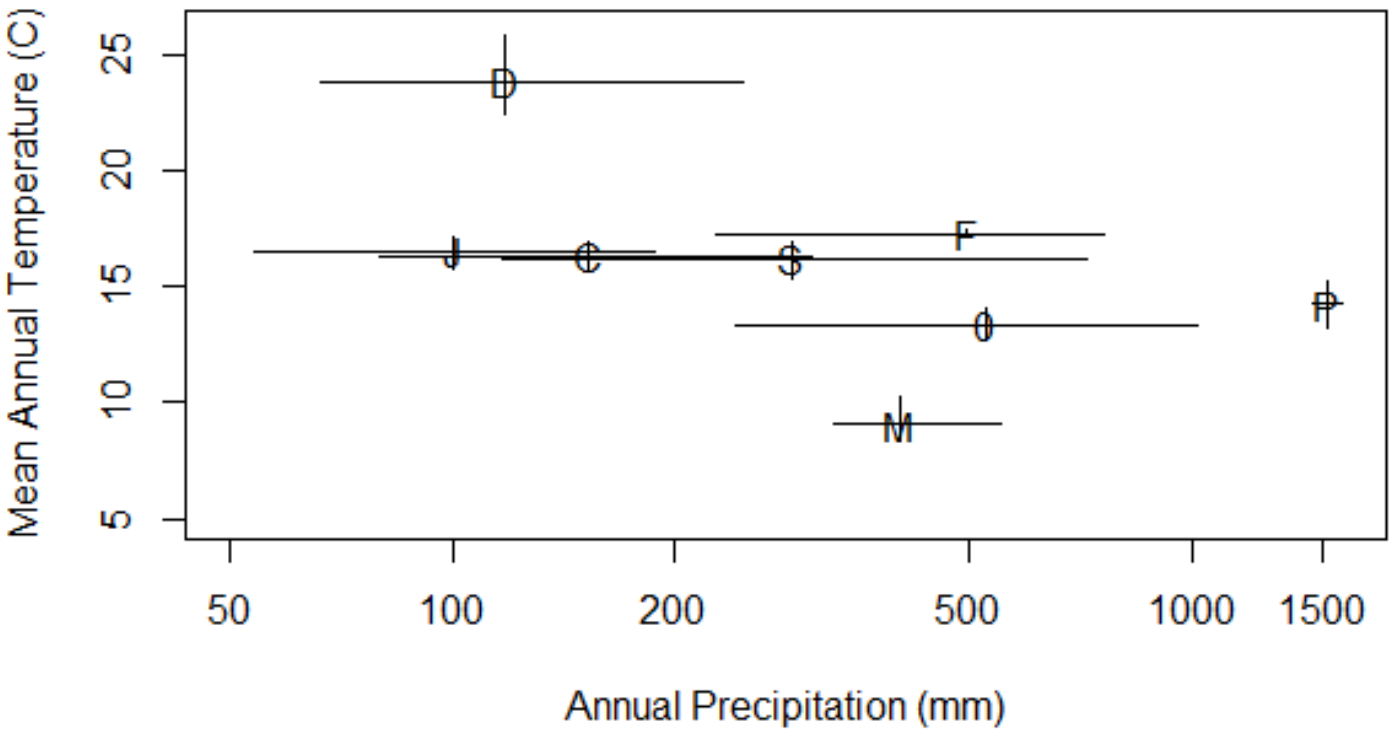

Figure 3: The range of annual mean temperatures and annual mean precipitation values recorded over the last several years at each site, including Desert (D), Pinyon-Juniper Woodland (J), Desert Chaparral (C), Coastal Sagebrush (same as Grassland) (S), Oak-Pine Forest (F), Ponderosa Pine (P), Oak-Pine Woodland (O), and Mixed Conifer Forest (M). The sites cover a wide range of climate types. The variability of annual precipitation is orders of magnitude larger than that of temperature.

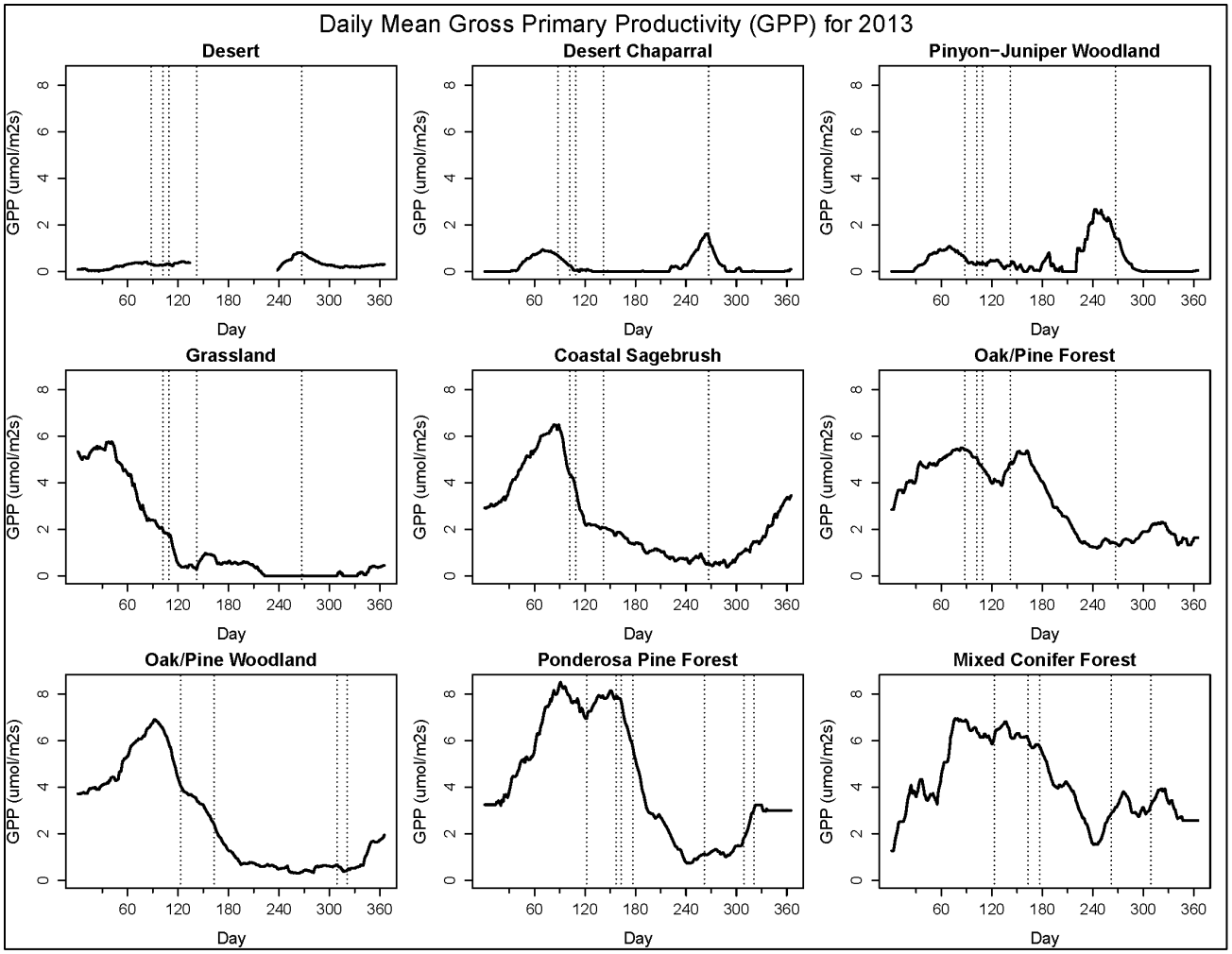

Figure 4: GPP for all sites from 2013 with AVIRIS imagery dates indicated by the vertical dashed line. GPP follows the precipitation regime, with maximums often following times of peak precipitation. The AVIRIS imagery captures a range of productivity levels for each site.

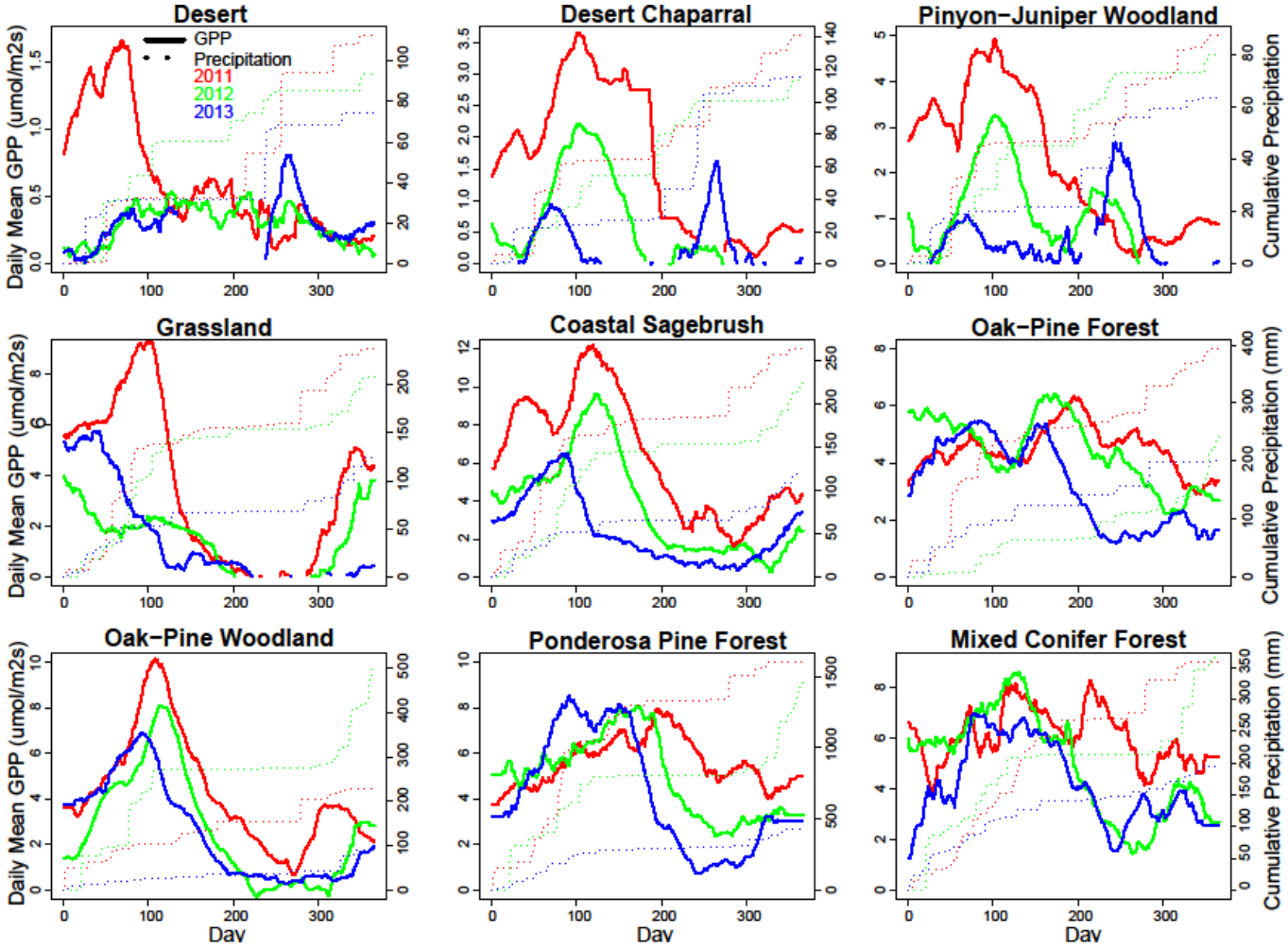

Figure 5: GPP and precipitation for sites our group visited in the field. All sites have seen a reduction in GPP since 2011 due to the persistent drought in California. The most extreme sites received 25% of 2011 precipitation in 2013. The oak/pine forest received more rain in 2013 than 2012, while the oak/pine woodland received more precipitation in 2012 than 2013. All other sites saw significant decreases in precipitation every year since 2011.

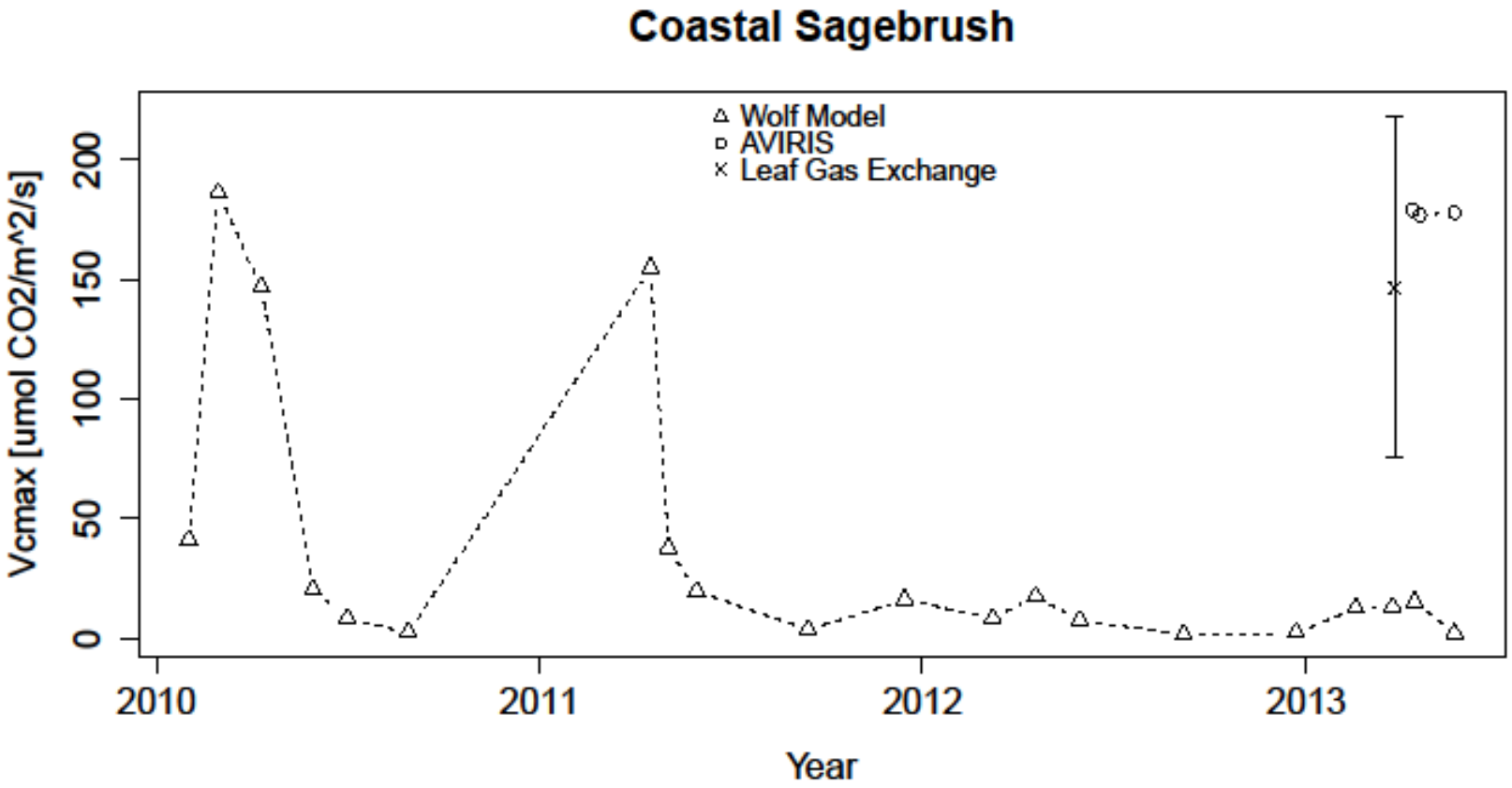

Figure 6: Vc_{max} values for the Coastal Sagebrush site, comparing estimates from the Wolf approach for modeling Vc_{max} from flux data and AVIRIS image, and measured field values for all dominant species. During drought conditions (2012 and 2013), the Wolf approach yields much lower estimates compared to pre-drought (2010 and 2011). However, the estimates from AVIRIS imagery are within the range measured in the field.

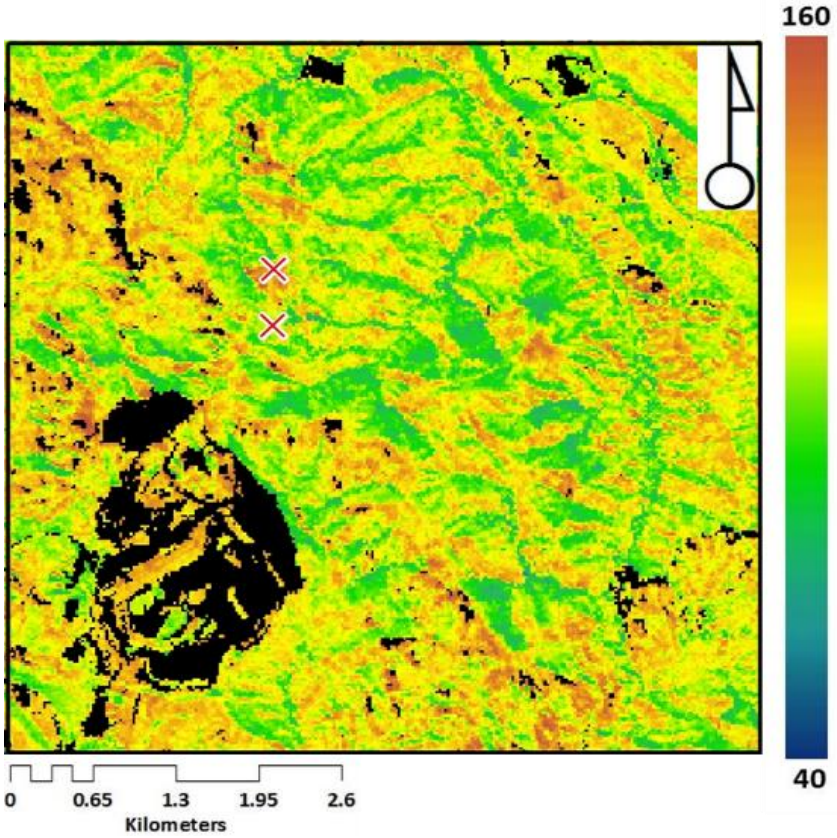

Figure 7: Map of Vc_{max} from 2013 spring for the Coastal Sagebrush (north red marker) and Grassland (south red marker) and the area around the sites. There is high variability in the photosynthetic parameter across the landscape, ranging from 70 to 140 µmol $CO_2/m^2/s$ for most of the region.

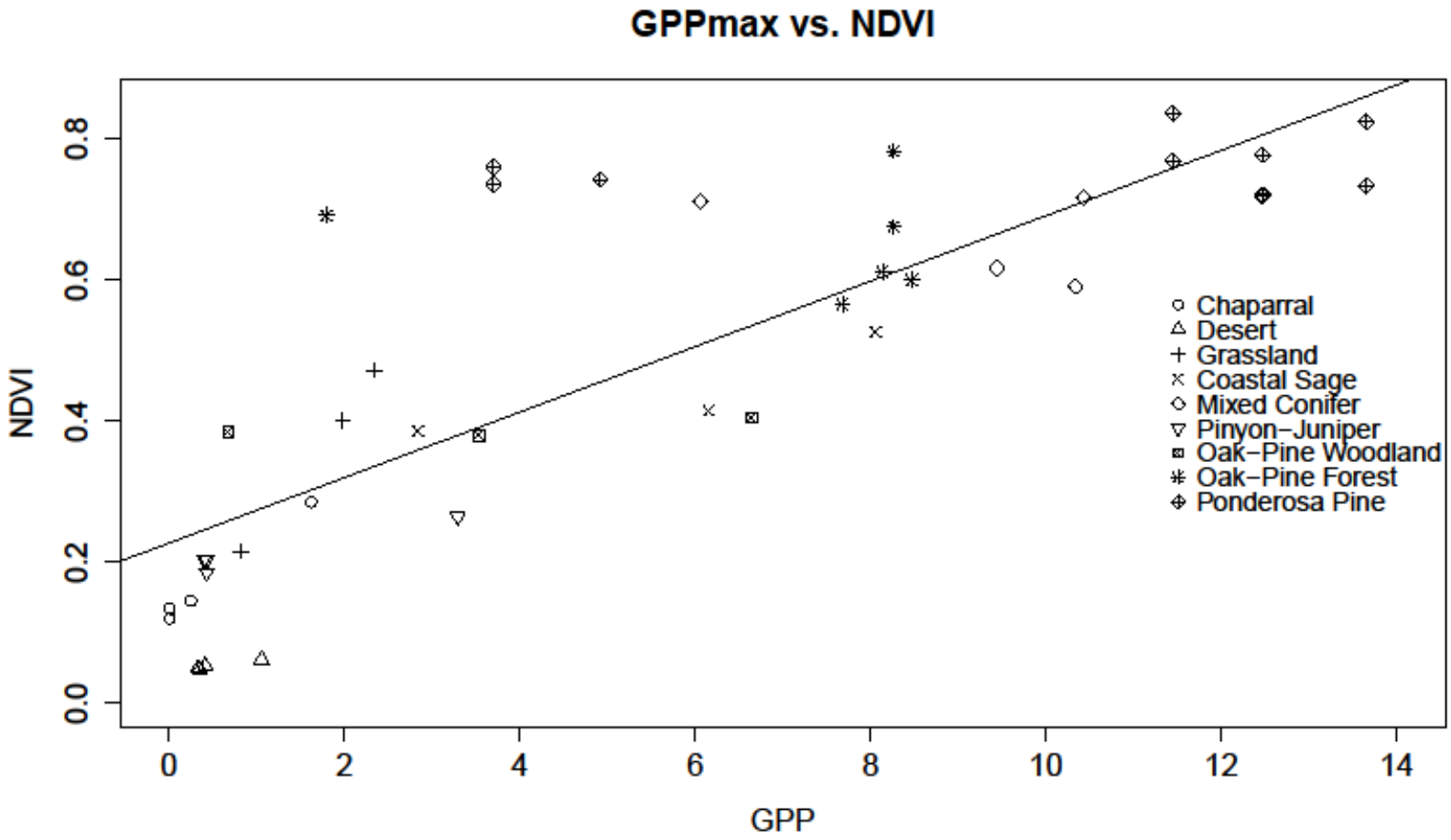

Figure 8: Plots of GPPmax vs. NDVI with linear regression lines. The trend inserted for all sites combined, resulting in a strong correlation between all sites. GPPmax is the maximum GPP value modeled for the site for a two week window around the overflight. GPP values are in µmol C/m^2/s.

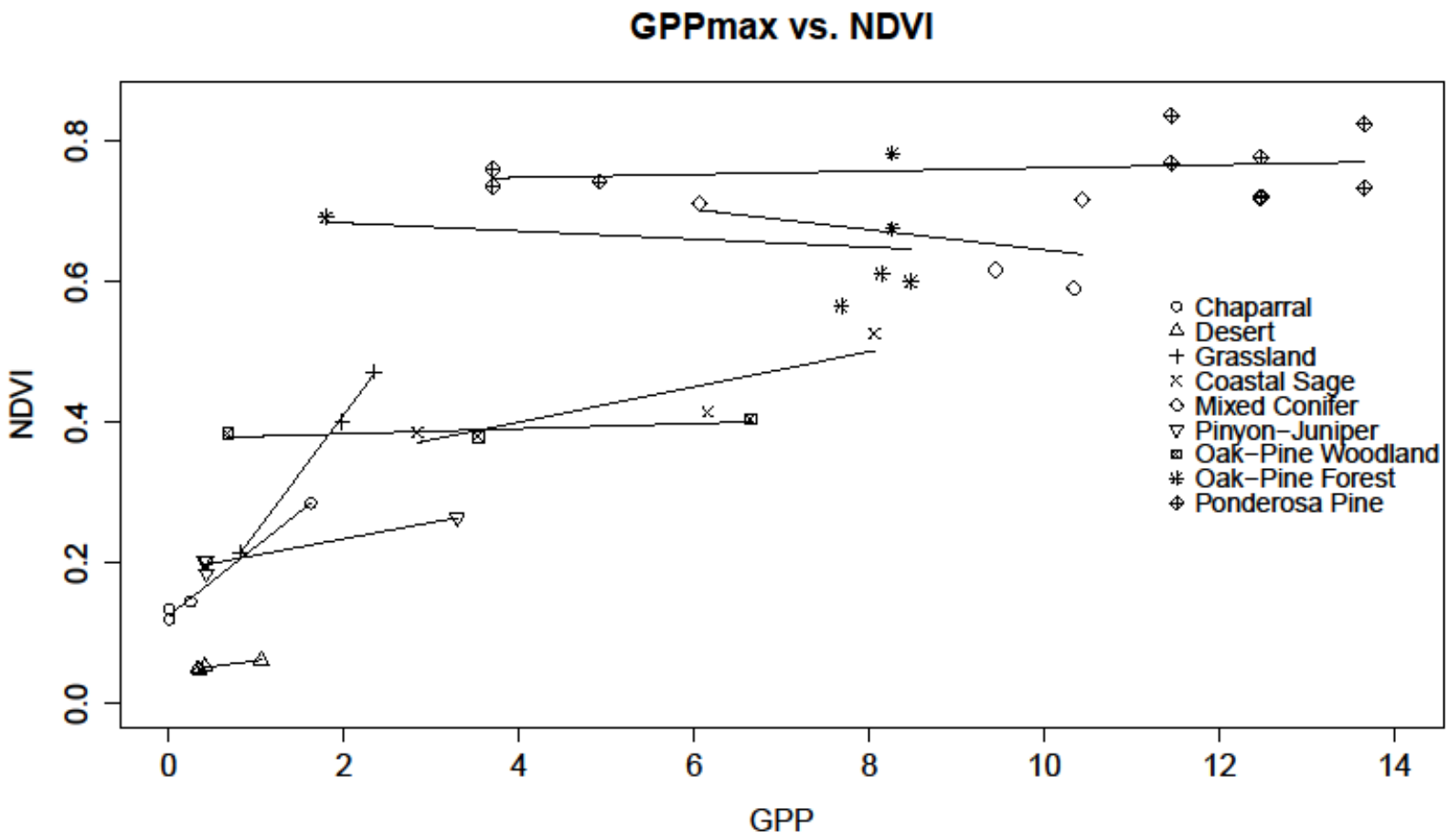

Figure 9: Plots of GPPmax vs. NDVI with linear regression lines. The trend is inserted per site, resulting in very weak to no correlation between GPP and NDVI within sites, especially for the forested sites with a full canopy. GPPmax is the maximum GPP value modeled for the site for a two week window around the overflight. GPP values are in µmol $C/m^2/s$.

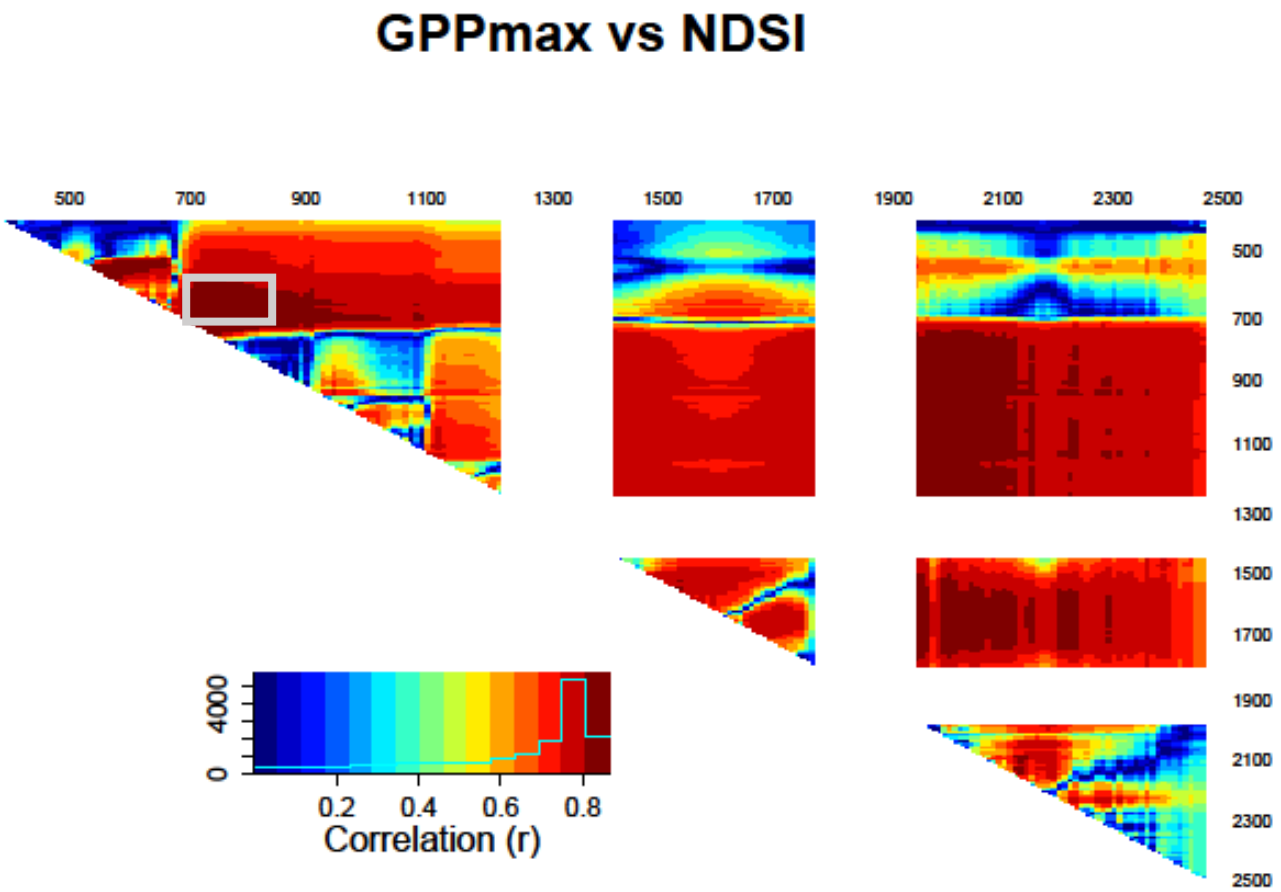

Figure 10: Heat map depicting indices of high correlation with GPPmax, with correlation histogram in bottom left of each figure. With all site data included, there are broad areas of high correlation, including NDVI area (outlined in gray box).

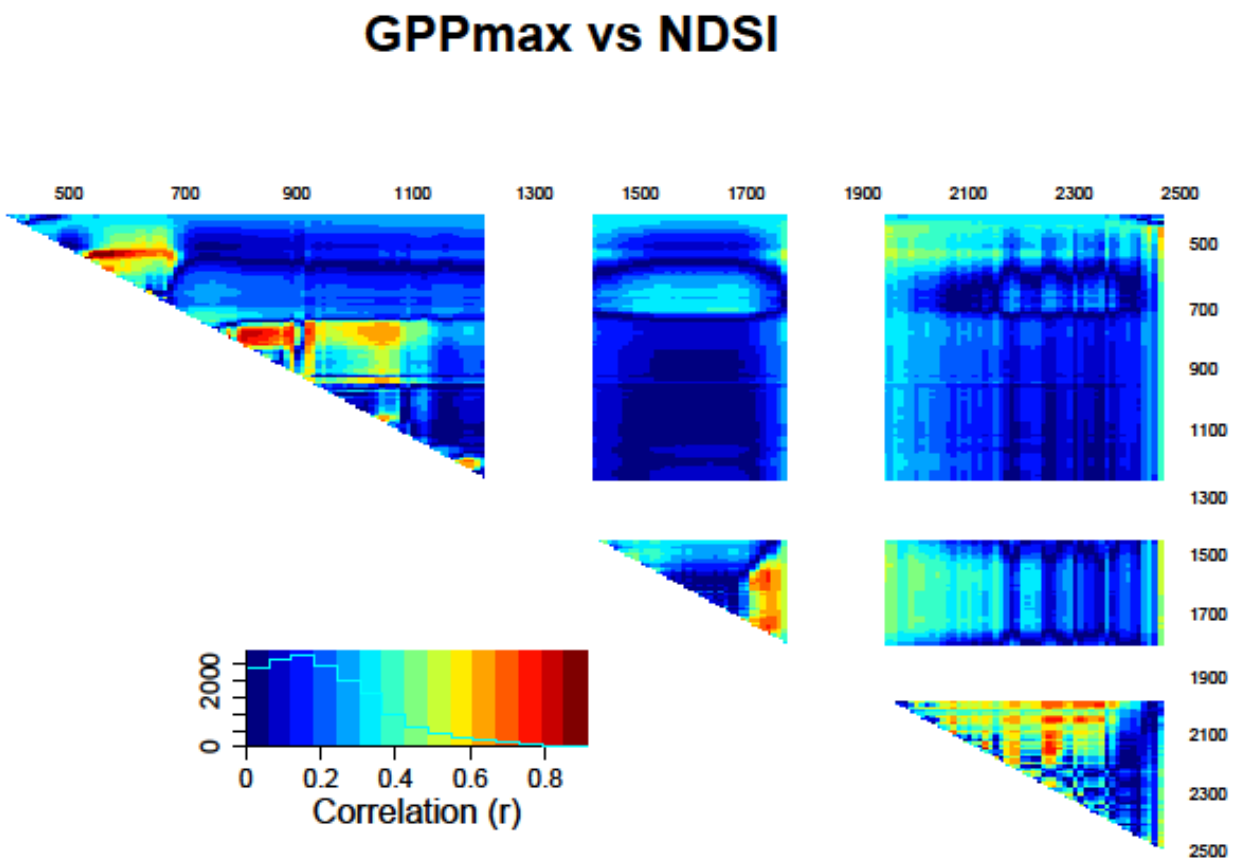

Figure 11: Heat map depicting indices of high correlation with GPPmax, with correlation histogram in bottom left of each figure. Confining the indices to mountain sites causes the broad areas of correlation drop out, while narrow band indices associated with specific features maintain high correlation.

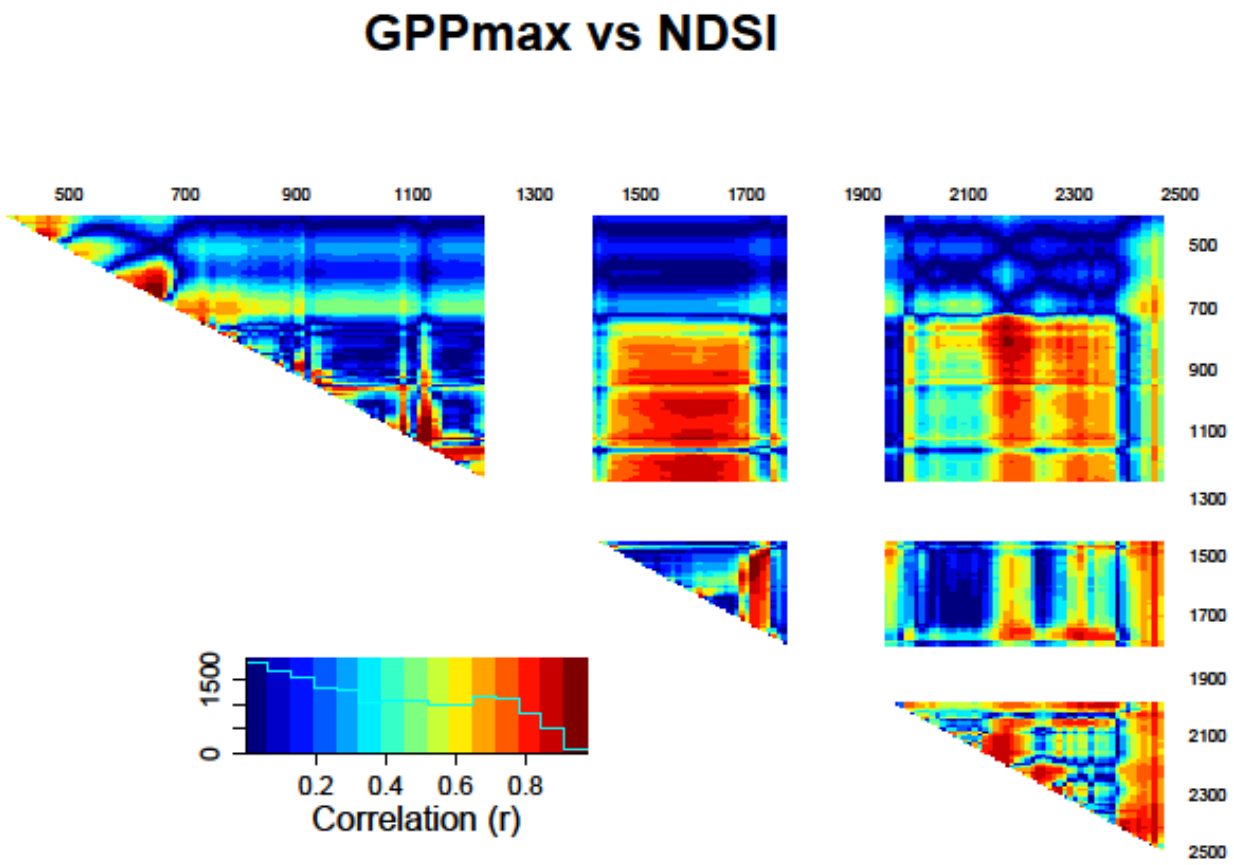

Figure 12: Heat maps depicting indices of high correlation with GPPmax for xeric sites, with correlation histogram in top left of each figure. Broad areas of correlation are removed for visible and NIR regions, but remain for indices composed of SWIR1 and NIR wavelengths, and portions of the SWIR 2 and NIR wavelengths.

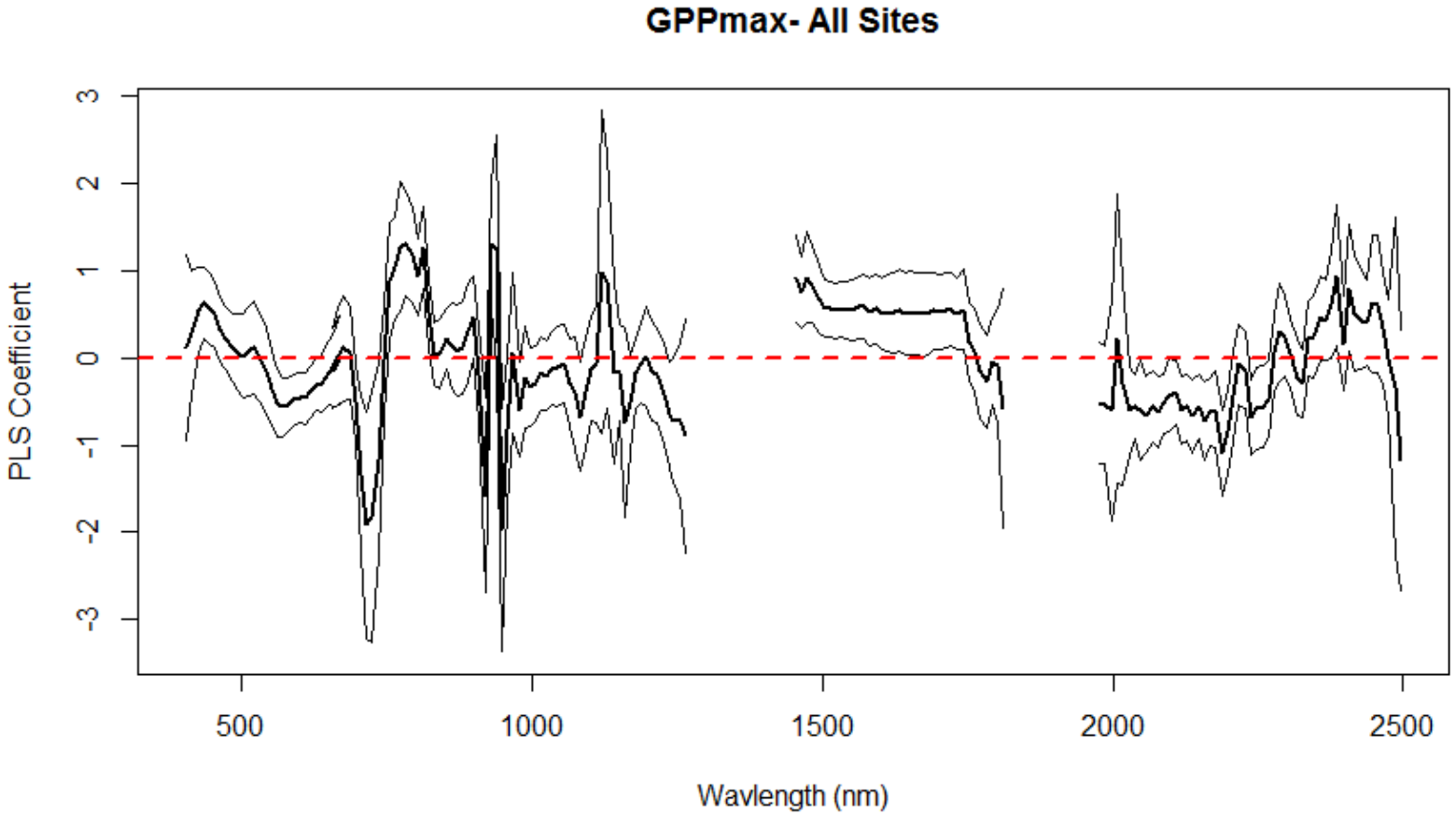

Figure 13: Plots of the mean standardized coefficients for each band and +/- 1 standard deviation based on the 100 model runs, for all sites. Wavelengths which have high importance in the model are often associated with known physiological features of the leaf.

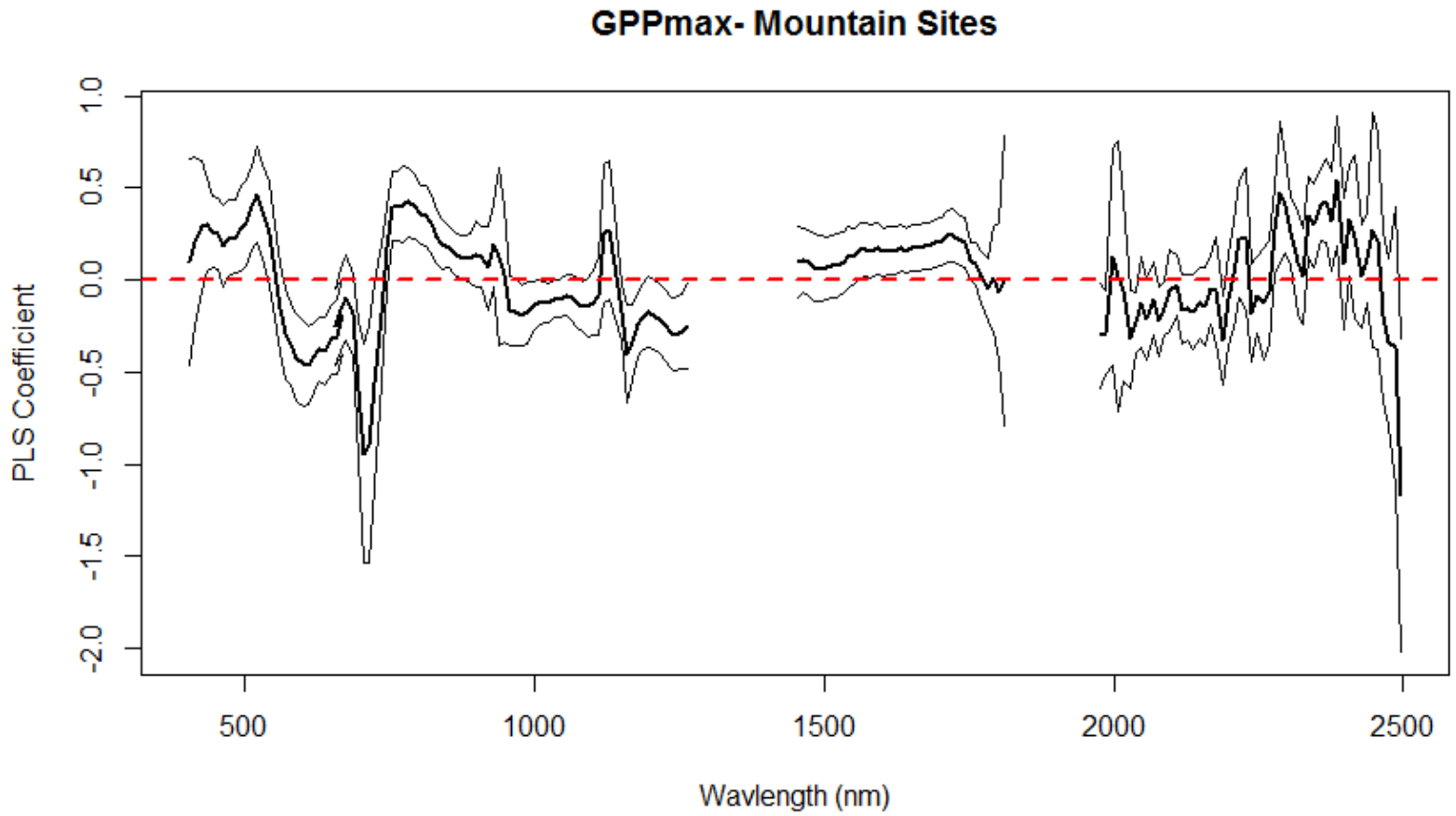

Figure 14: Plots of the mean standardized coefficients for each band and +/- 1 standard deviation based on the 100 model runs, for mountain sites only. Similar wavelengths have high importance in the model generated with all site data and the mountain sites subset, suggesting the wavelengths of high importance are associated with specific features present when examining across and within vegetation types.

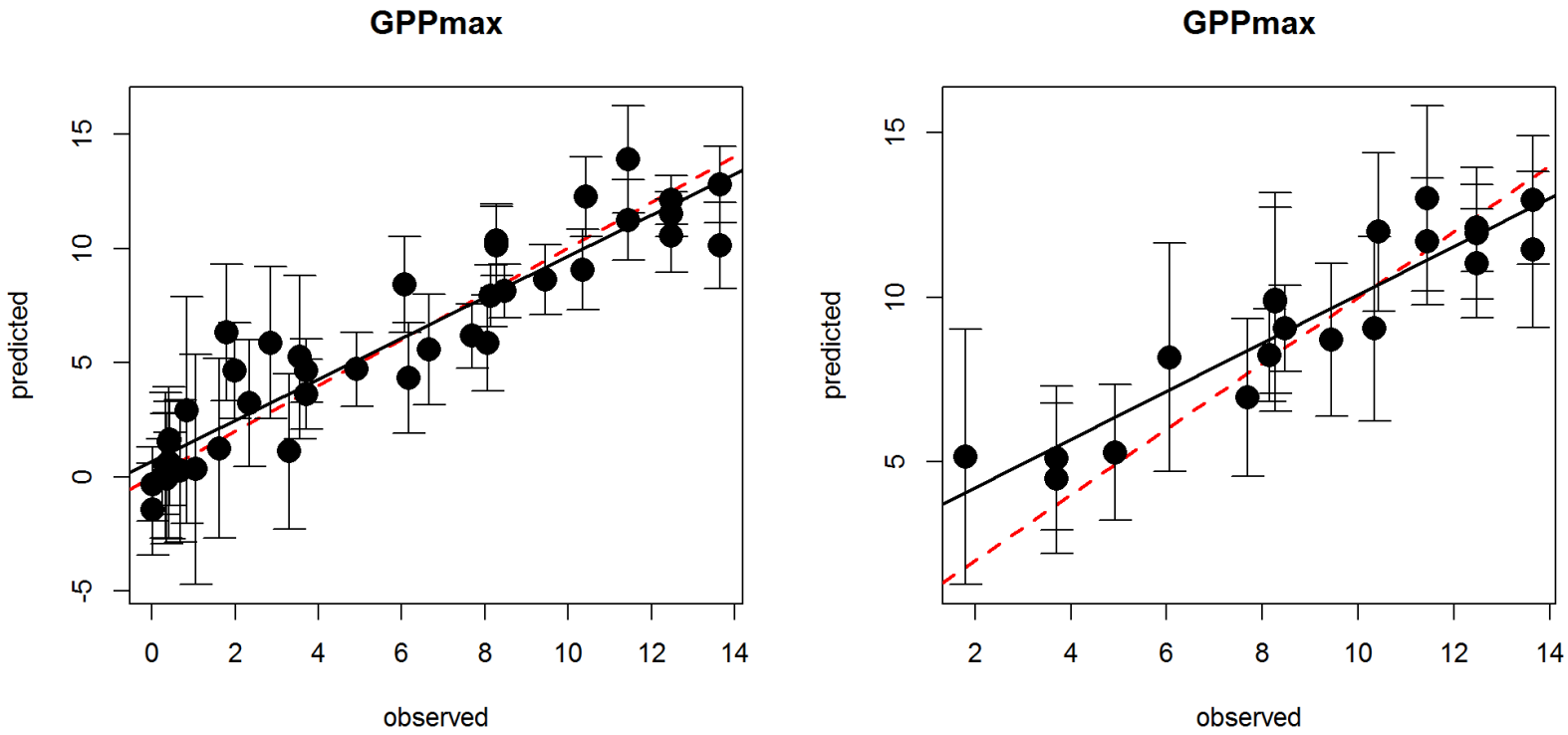

Figure 15: These figures present the predictive capabilities of the PLSR model generated with all site data (left) and with the mountain sites subset (right). While the mountain sites subset model has a larger bias as represented by the deviation of the black data-fitted line red dashed line indicating a 1:1 relationship, both models have strong predictive capabilities. Therefore, the PLSR model is able to estimate GPP within vegetation types over time, an area previous models using broad band remote sensing were poor. GPP values are in µmol $C/m^2/s$.

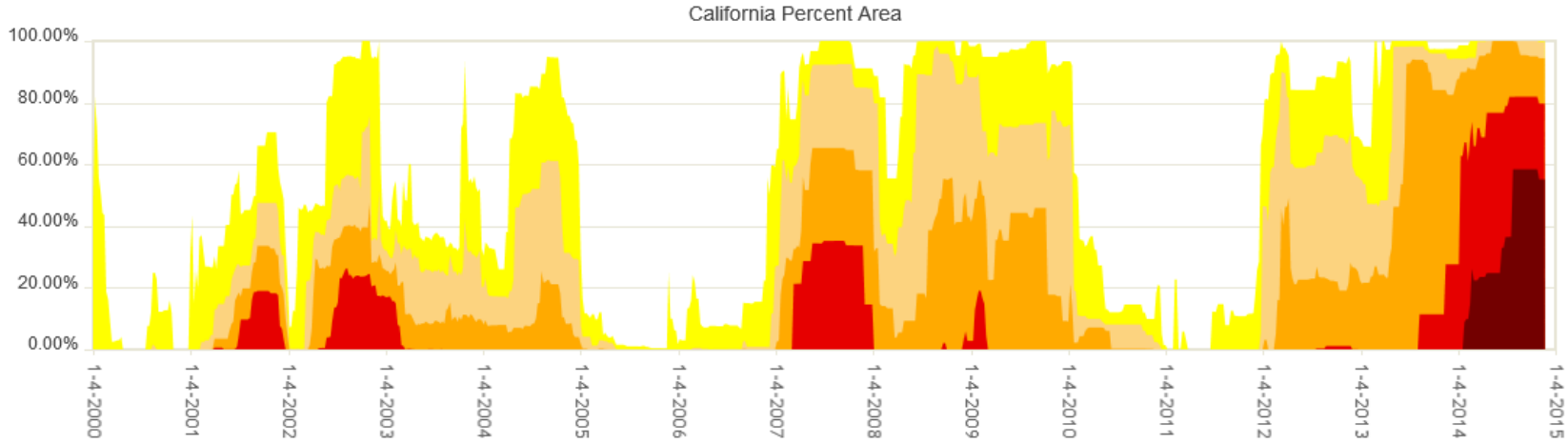

Figure 16: Cycles of wet and dry conditions characterize California climate over the past 15 years, with little to no drought in 2010 and 2011, and significant from 2012 onwards. US Drought Monitor- Dark red: Exceptional drought; Red: Extreme drought; Orange: Severe drought; Tan: Moderate drought. (National Drought Mitigation Center, 2014)

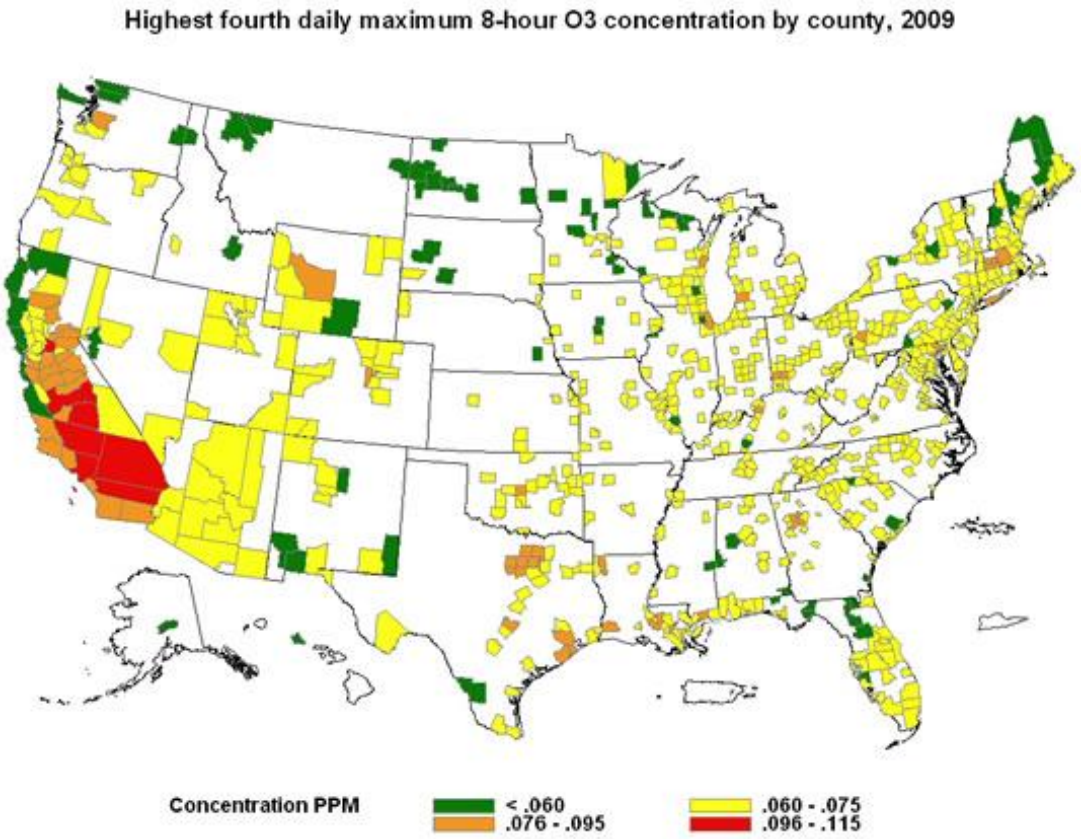

Figure 17: This map depicts ozone concentrations by county for 2009, showing where high ambient ozone concentrations were found in the United States. All orange and red areas exceeded the 8-hour air quality standard for ozone. Note the significant portion of California counties that exceeded the national standard in 2009. Although the map is from 2009, the same counties in California in non-attainment on this map often the ozone standard in 2013 as well. (Air Now, 2014)

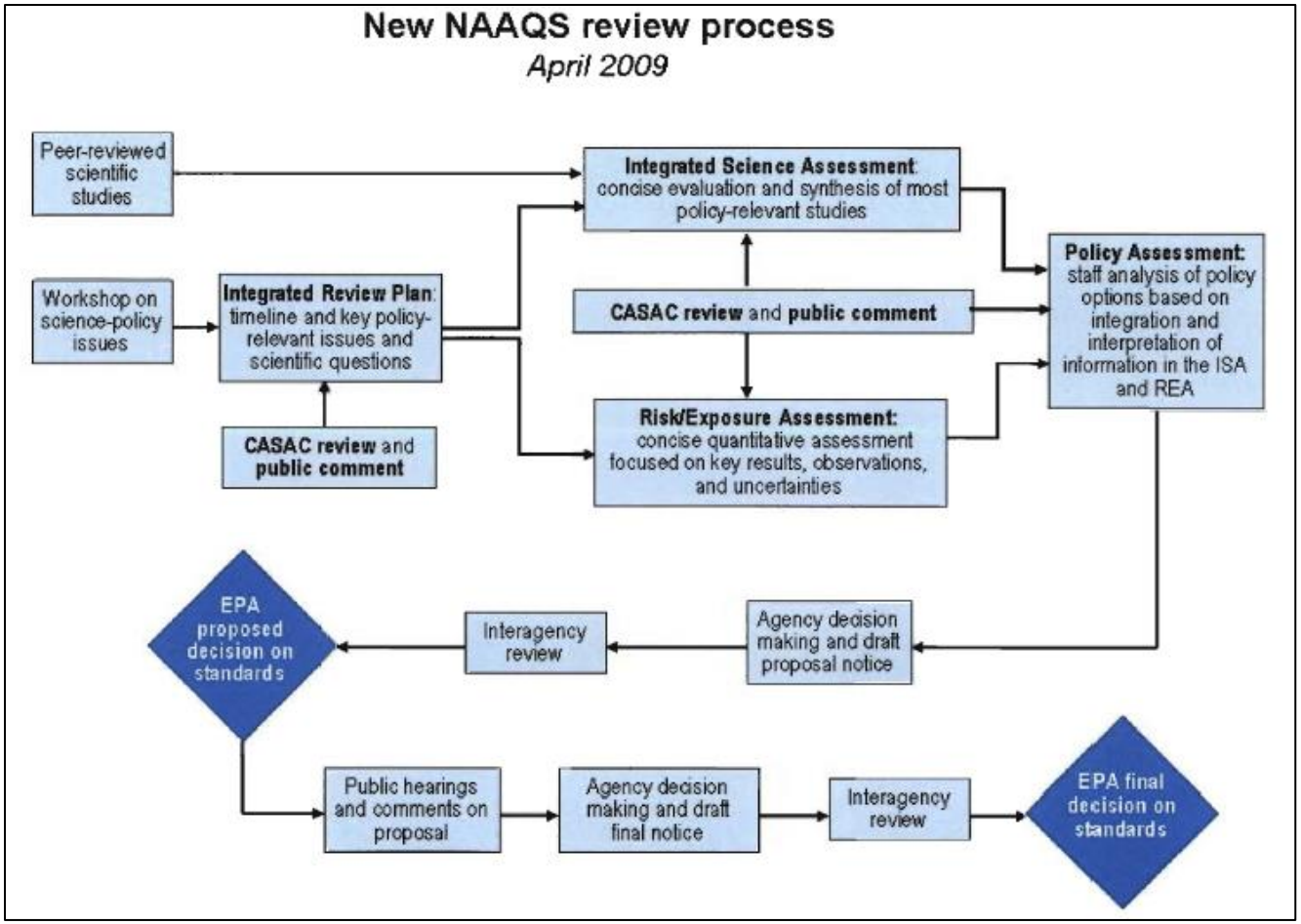

Figure 18: The major elements of the process for reviewing National Ambient Air Quality Standards. This process includes scientific and public review of the literature, with CASAC involved in generating a Policy Assessment after public comment, with a public review again occurring after the Administrator proposes to create new standards or maintain the current levels. (Jackson, 2009)